Journal of Computational Physics 227 (2008) 9428–9462

Contents lists available at ScienceDirect

Journal of Computational Physics

journal homepage: www.elsevier.com/locate/jcp

Towards a compact high-order method for non-linear hyperbolic systems, II. The Hermite-HLLC scheme

G. Capdeville *

Département de Mécanique des Fluides, Ecole Centrale de Nantes, 1, Rue de la Noe, B.P. 92101, 44321 Nantes cedex 3, France

ARTICLE INFO

Article history:
Received 21 March 2008
Received in revised form 19 June 2008
Accepted 25 June 2008
Available online 2 July 2008

Keywords:
Least-square reconstruction
Hermite polynomial
Weakly hyperbolic systems
δ-Shock waves
Dirac measure
Rankine–Hugoniot deficit
Monotonicity constraints

ABSTRACT

In a finite-volume framework, we develop an approximate HLL Riemann solver specific to weakly hyperbolic systems. Those systems are obtained by considering not only the variable but also its first spatial derivative, as unknowns. To this aim, we rely upon the theory of "δ-shock waves", newly developed in the scalar case.

First, we demonstrate that the extended version of the HLLE scheme to weakly hyperbolic systems is compatible with the existence of Dirac measures in the solution. Then, we develop a specific Hermite Least-Square (HLSM) interpolation that enables to generate a high-order and compact scheme, without creating spurious oscillations in the reconstruction of the variable or its first derivative. Extensive numerical experiments make it possible to validate the method and to check convergence to entropy solutions.

Relying upon those results, we construct a new HLL Riemann solver, suited for the extended one-dimensional Euler equations. For this purpose, we introduce the contribution of a contact discontinuity inside the definition of the solver. By using a formal analogy with the scalar study, we demonstrate that this solver tolerates the existence of "δ-shock waves" in the solution. Numerical experiments that follow help to validate some of the assumptions made to generate this scheme.

1. Introduction

In this paper, we develop a Riemann solver for a class of coupled hyperbolic systems of conservation laws. For that purpose, we rely upon the newly developed theory of "δ-shock waves".

Let us briefly recall this theory and its main results.

1.1. δ-Shock wave type solutions [1–6]

For some cases of coupled hyperbolic systems, "non-classical solutions" may occur when the Riemann problem does not possess a weak solution except for some particular initial data. In order to solve Cauchy problems in these situations, it becomes necessary to introduce new singularities called "δ-shocks", which are solution of the coupled hyperbolic systems.

To illustrate this problem, let us consider the following scalar non-linear conservation law:

$$u_t + f(u)_x = 0 \tag{1}$$

where, $f(u)$, is a convex smooth function, $f''(u) > 0$.

* Tel.: +33 2 4037 1651; fax: +33 2 4037 2523.
E-mail address: guy.capdeville@ec-nantes.fr

0021-9991/$ - see front matter © 2008 Elsevier Inc. All rights reserved.
doi:10.1016/j.jcp.2008.06.024

By differentiating this equation with respect to x and denoting $v \equiv u_x$, we obtain the following coupled hyperbolic system:

$$\begin{cases} u_t + f(u)_x = 0 \\ v_t + (f'(u)v)_x = 0 \end{cases} \tag{2}$$

System (2) is extremely degenerate – sometimes it is called "weakly hyperbolic" – with repeated eigenvalue $\lambda \equiv f'(u)$ and repeated eigenvector $(0,1)^t$. As a consequence, the linear component, v, of the solution, may contain Dirac measures while the non-linear component, u, preserves bounded variations.

If we consider the Cauchy problem for system (2), with the initial data

$$(u(x,t=0), v(x,t=0)) = \begin{cases} (u^l, v^l) & x < 0 \\ (u^r, v^r) & x > 0 \end{cases} \tag{3}$$

where $(u, v)^{l,\,r}$ are given constants, one can demonstrate that there are only two kinds of solutions for such a problem. The first one involves "δ-shock" waves, the second involves vacuums.

According to [5,7], the following theorem holds:

(a) if $u^l \geqslant u^r$, it exists a unique weak solution to the Cauchy problem (2) and (3). This solution has the following form:

$$\begin{cases} u(x,t) = u^l + [u] \times H(-x + x_s(t)) \\ v(x,t) = v^l + [v] \times H(-x + x_s(t)) - e(t) \times \delta(-x + x_s(t)) \end{cases} \tag{4}$$

Moreover, this solution satisfies the entropy condition

$$f'(u^l) \leqslant \frac{\mathrm{d}x_s}{\mathrm{d}t} \leqslant f'(u^r) \tag{5}$$

where we denoted: $[\cdot] \equiv (\cdot)^r - (\cdot)^l$, the jump of the variable u or v across the discontinuity. $H(x)$ is the Heaviside function and $\delta(x)$ is the delta function. In addition, functions $x_s(t)$ and $e(t)$ are defined by the system

$$\begin{cases} \frac{\mathrm{d}x_s}{\mathrm{d}t} = \frac{[f(u)]}{[u]}\Big|_{x=x_s(t)} \\ \frac{\mathrm{d}e}{\mathrm{d}t} = \left([f'(u)v] - [v]\frac{[f(u)]}{[u]}\right)\Big|_{x=x_s(t)} \end{cases} \tag{6}$$

with the initial data determined by (3) and $x_s(0) = 0$.

The solution (4) that satisfies (5) and (6), is called a "δ-shock" wave solution of the Cauchy problem (2) and (3). In this solution, the v component contains a δ measure while the u component is piecewise constant. The pair of equations defining (6) constitutes the "δ-shock Rankine–Hugoniot" conditions for the particular choice, (3).

The first equation of (6) is the standard Rankine–Hugoniot condition and gives the velocity of the δ-shock wave. This velocity verifies the classical entropy condition, (5), and means that all characteristics on both sides of the discontinuity, are in-coming.

The right-hand side of the second equation in (6) is less classical: it is called the "Rankine–Hugoniot deficit". In [8], it is demonstrated that the meaning of amplitude, $e(t)$, of δ-function in v, is the area under the graph $y = v(x_s(t), t)$.

Thus, the system of the Rankine–Hugoniot conditions, (6), determines the trajectory $x = x_s(t)$ of a δ-shock wave and the coefficient $e(t)$ of the singularity.

(b) If $u^l < u^r$, then, the weak solution to the Cauchy problem (2) and (3), is the following one, according to [7]:

$$(u(x,t), v(x,t)) = \begin{cases} (u^l, v^l) & x \leqslant f'(u^l) \times t \\ \left(\frac{x}{2t}, 0\right) & f'(u^l) \times t \leqslant x \leqslant f'(u^r) \times t \\ (u^r, v^r) & x \geqslant f'(u^r) \times t \end{cases} \tag{7}$$

In such a case, the first component, u, of solution (7), is the rarefaction wave while the second component, v, contains the intermediate "vacuum state": $v \equiv 0$.

In this article, we use those theoretical results to construct a HLL Riemann solver that is compatible with the existence of a δ-shock solution in (2).

1.2. Constructing a HLL Riemann solver for weakly hyperbolic systems

Recently, we developed a Hermite Least Square Monotone (HLSM) interpolation technique, in a finite-volume framework. This procedure aims at generating a compact high-order numerical method for systems of hyperbolic conservation laws [9]. For that purpose, we defined as discrete unknowns not only the primitive variable, u, but also its first spatial derivative, $v(\equiv u_x)$. Primitively, those two quantities are defined as solutions of a weakly hyperbolic system, identical to (2) and are evolved in time by using an approximate HLL Riemann solver, simply extended from [10].

Several numerical experiments confirmed the monotone behaviour and the accuracy properties of the resulting scheme. However, nothing was done in order to develop a "specific Riemann solver" that would be suited for weakly hyperbolic systems. In other words, we did not check the convergence towards the entropy solution, when the system is not strictly hyperbolic.

This limit may be detrimental, at least for two reasons: (i) we may need to use the first derivative – and therefore, the variable that presents a Dirac measure – either to interpolate the numerical solution or to calculate viscous stresses, with accuracy; (ii) δ-shocks can be related to realistic physical problems: for example, the "zero pressure gas dynamics" system is weakly hyperbolic ($v \geqslant 0$ and u are thought as the density and velocity variables, respectively). Similarly, systems that arise in non-linear geometric optics or in astrophysics are weakly hyperbolic and, therefore, may generate δ-shocks (see, for instance [6,11,12]).

For all these reasons, it becomes significant to ensure that a numerical method that necessitates solving a weakly hyperbolic problem, can incorporate into its main features, the mechanism that produces the appearance of a δ-shock type solution.

This way – even if the whole solution is not always mandatory – one may think that it will not exist numerical artefacts that would lessen or deteriorate the physical meaning of the numerical solution.

The study we propose in this article is organized in the following way: Section 2 presents an analysis of the weakly hyperbolic system, (2). First, we demonstrate that the extended version of the HLLE Riemann solver is compatible with the existence of δ-shocks into the numerical solution. Then, we modify the HLSM method [9], in order to capture solutions that present a Dirac measure. This point is achieved by adding a new constraint to the numerical least-square system. Lastly, the resulting scheme is validated on numerical test cases for which the exact solution is known. At this point, convergence towards the entropy solution is emphasized. In addition, we compare the modified HLSM method with a Hermite-WENO procedure [20].

In Section 3, we use these results to extend the scheme to the one-dimensional Euler equations for gas dynamics. To this aim, we develop a new version of the HLL scheme that discriminates between a shock-wave and a contact discontinuity. This way, a δ-shock may be correctly identified when it appears into the solution. We demonstrate, theoretically, this point and then, numerical experiments enable to prove the advantages gained from the new solver.

Finally, Section 4 summarizes the main results of this work and draws some conclusions and perspectives for a next future.

2. HLL Riemann solver for weakly hyperbolic systems: scalar case

2.1. Main theoretical results and notations

We write the scalar system (2), with its initial conditions, in the following vector form:

$$\begin{cases} U_t + F(U)_x = 0 \\ U(x, t=0) = U_o(x) \end{cases} \tag{8}$$

$$U \equiv [u, v]^t, F(U) \equiv [f(u), g(u, v)]^t \quad (f'' > 0)$$

with:

$$U_o \equiv [u_o, v_o]$$

where we defined: $\begin{cases} g(u, v) \equiv f'(u) \times v \equiv a(u) \times v \\ v_o(x) \equiv \frac{\mathrm{d}}{\mathrm{d}x} u_o(x) \end{cases}$ $g(u, v)$ is a smooth function, linear with respect to v.

By defining the Jacobian matrix, $A(U) \equiv \frac{\partial F}{\partial U}$, system (8) can be written, equivalently, as

$$\begin{cases} U_t + A(U) \times U_x = 0 \\ U(x, t=0) = U_o(x) \end{cases} \tag{9}$$

$$\text{with :} \quad A(U) \equiv \begin{bmatrix} a(u) & 0 \\ a'(u)v & a(u) \end{bmatrix} \tag{10}$$

Obviously, this system is weakly hyperbolic: it has a double eigenvalue and only one right eigenvector

$$\lambda \equiv a(u), \quad r \equiv [0, 1]^t \tag{11}$$

The system is also non-diagonalizable in v. The associated system of characteristic equations can be written as

$$\begin{cases} \frac{\mathrm{d}x}{\mathrm{d}t} = a(u) \\ \frac{\mathrm{d}u}{\mathrm{d}t} = 0 \\ \frac{\mathrm{d}v}{\mathrm{d}t} = -a'(u)vu_x = -a'(u)v^2 \end{cases} \tag{12}$$

demonstrating that the characteristic curves are straight lines and that u remains constant along each of them. If we consider (8) or (9) with sufficiently smooth data, the exact solution can be obtained from (12). Indeed, the characteristic passing through any given point $x_0 \equiv x(t=0)$ on the x-axis, is

$$x = x_0 + a(u_0(x_0)) \times t \tag{13}$$

Then, along this characteristic, the exact solution of (9) is such that

$$\begin{cases} u(x,t) = u_0(x - a(u_0(x_0)) \times t) \\ v(x,t) = \frac{v_0(x_0)}{1 + a'(u_0(x_0)) \times v_0(x_0) \times t} \end{cases} \tag{14}$$

If there are regions where $u_0'(x_0) < 0$, then the smooth solution of (9) is defined by

$$(u,v)(x,t) = \left(u_0(x_0), \frac{v_0(x_0)}{1 + a'(u_0(x_0)) \times v_0(x_0) \times t} \right) \tag{15}$$

only for $t < -(a'(u_0(x_0)) \times v_0\,(x_0))^{-1}$.

For a *bounded* discontinuity located at $x = \sigma t$, the Rankine–Hugoniot condition holds: $-\sigma[U] = [F(U)]$; or in a more expanded form:

$$\begin{cases} -\sigma[u] + [f(u)] = 0 \\ -\sigma[v] + [a(u)v] = 0 \end{cases} \tag{16}$$

where $\sigma(\equiv \mathrm{d}x/\mathrm{d}t)$ is the propagation speed of the discontinuity and $[\cdot] \equiv (\cdot)^r - (\cdot)^l$ represents the jump across this discontinuity.

Solving (16), two possibilities arise. First, if $[u] = 0$, the only solution for σ is then:

$$\sigma = a(u^l) = a(u^r) \tag{17}$$

This solution is a contact discontinuity in v; it is just the characteristic line that connects the states (u^l,v^l) and (u^r,v^r).

Now, in the case $u^l > u^r$ and, therefore, $a(u^l) > a(u^r)$ – because of the monotonicity of $a(u)$ – it is easy to infer from (12), that the characteristic lines will overlap at a finite time: in such a case a discontinuity must appear. However, this discontinuity is not a classical weak solution of (9): it develops a Dirac measure in a finite time, although the initial data $(u_0, v_0)(x)$ are smooth. This property can be illustrated by solution (15). Indeed, in regions where $u_0'(x_0) < 0$, we obtain the following result:

$$(u,v)(x,t) \xrightarrow[t \to -(a'(u_0(x_0)) \times v_0(x_0))^{-1}]{} (u_\sigma, \infty) \tag{18}$$

with the entropy condition [6]: $u^l > u_\sigma > u^r$.

Consequently, the linear component, v, of the solution, becomes singular. In order to solve the Cauchy problems in those "no classical" situations, it is necessary to introduce new singularities called "δ-shocks", which are solution of (8) or (9). More precisely, one can demonstrate that the solution of the Riemann problem

$$U_0(x) = \begin{cases} (u^l, v^l) x < 0 \\ (u^r, v^r) x > 0 \end{cases} \quad (u^l > u^r)$$

associated to (9), is the following one [5]:

$$\begin{cases} u(x,t) = u^l + [u] \times H(x - \sigma t) \\ v(x,t) = v^l + [v] \times H(x - \sigma t) - e(t) \times \delta(x - \sigma t) \end{cases} \tag{19}$$

with the following entropy condition for δ-shocks:

$$a(u^l) \geqslant \sigma \geqslant a(u^r) \tag{20}$$

and the generalized Rankine–Hugoniot conditions defining σ and $e(t)$:

$$\begin{cases} \sigma \equiv \left. \frac{[f(u)]}{[u]} \right|_{x=\sigma t} \\ e(t) \equiv ([a(u)v] - \sigma \times [v])|_{x=\sigma t} \times t \end{cases} \tag{21}$$

Now, σ represents the propagation speed of the δ-shock wave and $e(t)$ is called the "Rankine–Hugoniot deficit". This latter term can be interpreted as the error introduced into the solution by considering that the discontinuity in the linear variable, v, propagates at the same speed, σ, as the discontinuity for u.

Indeed, the Rankine–Hugoniot condition, $\sigma = [a(u)v]/[v]$, cannot be simultaneously verified with the first condition, $\sigma = [f(u)]/[u]$, when $[u] \neq 0$. Therefore, it exists a deficit into the Rankine–Hugoniot condition, for the variable, v. Solution (19) shows us that this deficit is necessarily propagated along the discontinuity path, $x = \sigma \times t$. $e(t)$ is proportional to the difference between the velocity for the discontinuity in u and that for the discontinuity in v.

One can also demonstrate [8], that this term has a geometrical meaning: it represents the increase in time of the total area under the graph $y = v(\sigma t,\ t)$. Solution (19) can be extended to the fluxes $(f,\ g)(x,\ t)$, to produce the following useful result:

$$\begin{cases} f(u(x,t)) = f(u^l) + [f(u)] \times H(x - \sigma t) \\ g(u,v)(x,t) = g(u^l, v^l) + [a(u)v] \times H(x - \sigma t) - e(t) \times \sigma \times \delta(x - \sigma t) \end{cases} \tag{22}$$

In what follows, we use Eqs. (19) and (21) and (22) to check the properties of the extended version of the HLLE scheme discretizing system (8).

2.2. HLLE scheme for a weakly hyperbolic system

To study the behaviour of the HLLE scheme, we consider the following modified form of system (9):

$$\begin{cases} U_t + A_\varepsilon(U) \times U_x = 0 \\ A_\varepsilon(U) \equiv \begin{bmatrix} a(u) & 0 \\ a'(u)v & a(u) + \varepsilon \end{bmatrix} \quad (0 < \varepsilon \ll 1) \end{cases} \tag{23}$$

Now, this system is strictly hyperbolic since its eigenvalues are

$$\lambda_1(u) \equiv a(u); \quad \lambda_2(u) \equiv a(u) + \varepsilon \tag{24}$$

Let us investigate an approximate solution of the Riemann problem for system (23).

To get this solution, we decide to extend to (23), the HLL scheme defined in [10]. In such a case, the solution of the Riemann problem is approximated according to Fig. 1. The intermediate state, U^*, is calculated according to the following result:

$$U^* = \frac{\lambda_\varepsilon^r U^r - \lambda^l U^l + F(U^l) - F(U^r)}{\lambda_\varepsilon^r - \lambda^l} \tag{25}$$

And the intermediate flux, F^*, is deduced by using the Rankine–Hugoniot condition across the wave $x = \lambda^l t$ or $x = \lambda_\varepsilon^r t$:

$$F^* = F(U^l) + \lambda^l(U^* - U^l) = F(U^r) + \lambda_\varepsilon^r(U^r - U^*) = \frac{\lambda_\varepsilon^r F(U^l) - \lambda^l F(U^r) + \lambda_\varepsilon^r \lambda^l (U^r - U^l)}{\lambda_\varepsilon^r - \lambda^l} \tag{26}$$

If we define the wave speeds, λ^l and λ_ε^r, as

$$\lambda^l \equiv \min(a^l, \hat{a})$$
$$\lambda_\varepsilon^r \equiv \max(a^r, \hat{a}) + \varepsilon$$

with $a^{l,\,r} \equiv a(u^{l,r})$ and $\hat{a} \equiv \begin{cases} \frac{(f(u^l) - f(u^r))}{u^l - u^r} & if u^l \neq u^r \\ a^l \text{ otherwise} \end{cases}$ then, we constructed a HLLE scheme, suited in discretizing (23).

Therefore, using those results, one can define the generalized approximate solution for the Riemann problem associated to system (23). For $U_\varepsilon(x,\ t)$, solution of (23), we have

$$U_\varepsilon(x,t) = \begin{cases} (u^l, v^l) & x < \lambda^l t \\ (u^*, v^*) & \lambda^l t \leqslant x \leqslant \lambda_\varepsilon^r t \\ (u^r, v^r) & x > \lambda_\varepsilon^r t \end{cases} \tag{27}$$

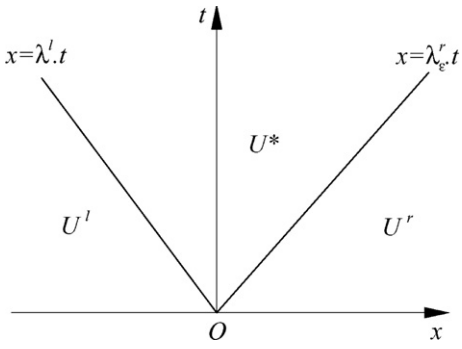

Fig. 1. HLL solution for a weakly hyperbolic system.

And for the flux, $F_\varepsilon(x,t)$:

$$F_\varepsilon(x,t)=\begin{cases}(f(u^l),g(u^l,v^l)) & x<\lambda^l t\\ (f^*,g^*) & \lambda^l t\leqslant x\leqslant\lambda_\varepsilon^r t\\ (f(u^r),g(u^r,v^r)) & x>\lambda_\varepsilon^r t\end{cases}\tag{28}$$

To begin this analysis, *let us suppose that* $u^l < u^r$.

Then, the entropy solution for (23) is a rarefaction wave for the variable, u. Accordingly, we have $\lambda^l = a^l$ and $\lambda_\varepsilon^r = a^r + \varepsilon$.

Consequently, using this result into (25) and inserting into (27), one can finally write:

$$U(x,t)\equiv\lim_{\varepsilon\to0^+}U_\varepsilon(x,t)=\begin{cases}(u^l,v^l) & x<a^l t\\ (u^*,0) & a^l t\leqslant x\leqslant a^r t\\ (u^r,v^r) & x>a^r t\end{cases}\tag{29}$$

with: $u^*=\frac{a^r u^r-a^l u^l+f(u^l)-f(u^r)}{a^r-a^l}$.

This solution represents the correct approximate solution of (7) and u^* is the averaged value of the rarefaction fan centred at the origin for the non-linear variable, u.

Now, *suppose that* $u^l > u^r$.

According to the results presented in [5,8], we know that a δ-shock wave appears in the solution. Then, we have: $\lambda^l=\hat{a}$ and $\lambda_\varepsilon^r=\hat{a}+\varepsilon$.

In such a case, formulae (25) and (26) give the following results:

$$U^*=\begin{cases}u^r\\ v^r+\frac{\hat{a}[v]-[g]}{\varepsilon}\end{cases},\quad F^*=\begin{cases}f(u^r)\\ g(u^l,v^l)+\hat{a}[v]+\hat{a}\times\frac{(\hat{a}[v]-[g])}{\varepsilon}\end{cases}\tag{30}$$

Using those results into (27) and (28), one can write, equivalently

$$\begin{cases}U_\varepsilon(x,t)=U^l+(U^*-U^l)\times H(x-\hat{a}t)+(U^r-U^*)\times H(x-(\hat{a}+\varepsilon)\times t)\\ F_\varepsilon(x,t)=F(U^l)+(F^*-F(U^l))\times H(x-\hat{a}t)+(F(U^r)-F^*)\times H(x-(\hat{a}+\varepsilon)\times t)\end{cases}\tag{31}$$

Consequently, when $\varepsilon\to0^+$, we obtain:

$$\lim_{\varepsilon\to0^+}U_\varepsilon(x,t)=\begin{cases}u^l+[u]\times H(x-\hat{a}t)\\ v^l+[v]\times H(x-\hat{a}t)+(\hat{a}[v]-[g])\times\lim_{\varepsilon\to0^+}\frac{\{H(x-\hat{a}t)-H(x-(\hat{a}+\varepsilon)t)\}}{\varepsilon}\end{cases}\tag{32}$$

Using the property: $\lim_{\varepsilon\to0^+}\frac{\{H(x-\hat{a}t)-H(x-(\hat{a}+\varepsilon)t)\}}{\varepsilon}=t\times\delta(x-\hat{a}t)$ (Dirac function), we get the following result:

$$U(x,t)=\begin{cases}u^l+[u]\times H(x-\hat{a}t)\\ v^l+[v]\times H(x-\hat{a}t)-([g]-\hat{a}[v])\times t\times\delta(x-\hat{a}t)\end{cases}\tag{33}$$

Since $\hat{a}\equiv\sigma$ and using the convexity of flux f, we can deduce that the entropy condition (20) is ensured. Consequently, solution (33) is identical to the exact solution, (19).

Similarly, we obtain the following result for the flux function, $F(x,t)\equiv\lim_{\varepsilon\to0^+}F_\varepsilon(x,t)$:

$$F(x,t)=\begin{cases}f(u^l)+[f]\times H(x-\hat{a}t)\\ g(u^l,v^l)+[g]\times H(x-\hat{a}t)-\hat{a}([g]-\hat{a}[v])\times t\times\delta(x-\hat{a}t)\end{cases}\tag{34}$$

This latter solution is identical to (22).

Therefore, the extended version of the HLLE scheme to weakly hyperbolic systems is compatible with the existence of δ-shocks into the solution.

Remark 1. Practically, the Dirac measure in the variable v does not hold in the computation of the numerical flux. Indeed, if we discretize (8) by a finite-volume method, we must evaluate the numerical flux, $F_{i+1/2}(t)$, at the interfaces $x = x_{i+1/2}$ and near the axis $t = t_n$. In this case, formula (34) can be re-written as

$$F_{i+1/2}(t)=\begin{cases}f(u^l)+[f]\times H(-\hat{a}(t-t_n))\\ g(u^l,v^l)+[g]\times H(-\hat{a}(t-t_n))-\hat{a}([g]-\hat{a}[v])\times(t-t_n)\times\delta(-\hat{a}(t-t_n))\end{cases}\tag{35}$$

The Dirac term has an influence only if the discontinuity line $x=\hat{a}(t-t_n)$ coincides with the axis $x = x_{i+1/2}$, or in other words, if $\hat{a}=0$. However, in such a case, the singularity into the calculation of $g_{i+1/2}(t)$ must disappear according to the following property:

$$\hat{a}\times\delta(\hat{a}(t-t_n))\underset{\hat{a}\to0}{\to}0\tag{36}$$

Remark 2. The eigenvalues, $\lambda^{l,r}$, defining the HLLE scheme, are constructed with reference to the non-linear variable, u. One could have decided to construct those eigenvalues from the linear variable, v, by defining the propagation speed of the discontinuity, $\hat{a}$, with the Rankine–Hugoniot condition

$$\hat{a} \equiv \frac{[g]}{[v]} = \frac{g(u^r, v^r) - g(u^l, v^l)}{v^r - v^l} \tag{37}$$

However, this choice would not ensure that the entropy condition is satisfied. Indeed, condition (20) is not necessarily satisfied by (37) because the flux $g(u,v)$ is not necessarily a convex function of u.

Remark 3. The version of the HLLE scheme we derived in order to discretize system (8) is equivalent to the construction of a Roe's scheme for this system.

Let us briefly demonstrate this point.

The Roe's average that linearizes system (23) is calculated by defining the constant matrix, $\hat{A}_\varepsilon$, which verifies the conservativity conditions

$$[F_\varepsilon] = \hat{A}_\varepsilon [U] \tag{38}$$

where we set: $F_\varepsilon \equiv \partial \hat{A}_\varepsilon / \partial U$.

If we define $\hat{A}_\varepsilon$ in agreement with the form of $A(U)$ in (23), we shall write $\hat{A}_\varepsilon$ as

$$\hat{A}_\varepsilon \equiv \begin{bmatrix} \hat{a} & 0 \\ \hat{b}_\varepsilon & \hat{a} + \varepsilon \end{bmatrix} \tag{39}$$

Then system (38) using definition (39), can be solved for the unknowns $(\hat{a}, \hat{b}_\varepsilon)$ to give the following result:

$$\begin{cases} \hat{a} = \frac{[f]}{[u]} \\ \hat{b}_\varepsilon = ([a(u)v] - (\hat{a} + \varepsilon)[v])/[u] \end{cases} \tag{40}$$

Once $\hat{A}_\varepsilon$ is calculated, one can formulate its eigenvalues and right eigenvectors. Thus, we obtain the following results:

$$\begin{cases} \hat{\lambda}_1 = \hat{a}, \hat{r}_1 = [\varepsilon, -\hat{b}_\varepsilon]^t \\ \hat{\lambda}_2 = \hat{a} + \varepsilon, \hat{r}_2 = [0, 1]^t \end{cases} \tag{41}$$

Finally, the associated wavestrengths $(\hat{\alpha}_1, \hat{\alpha}_2)$ can be calculated to give:

$$\begin{cases} \hat{\alpha}_1 = \frac{1}{\varepsilon}[u] \\ \hat{\alpha}_2 = \frac{1}{\varepsilon}\left(\hat{b}_\varepsilon [u] + \varepsilon [v]\right) \end{cases} \tag{42}$$

Consequently, any fluctuation $[U] = U^r - U^l$, can be decomposed along each linearized wave, according to:

$$[U] = \frac{1}{\varepsilon}[u] \times \begin{bmatrix} \varepsilon \\ -\hat{b}_\varepsilon \end{bmatrix} + \frac{1}{\varepsilon}\left(\hat{b}_\varepsilon [u] + \varepsilon [v]\right) \times \begin{bmatrix} 0 \\ 1 \end{bmatrix} \tag{43}$$

Therefore, we can formulate the generalized solution, $U_\varepsilon(x,t)$, of (23) close to $x = x_{i+1/2}$, $t = t_n$:

$$U_\varepsilon(x,t) = U^l + \frac{1}{\varepsilon}[u] \times \begin{bmatrix} \varepsilon \\ -\hat{b}_\varepsilon \end{bmatrix} \times H\left[(x - x_{i+1/2}) - \hat{a}(t - t_n)\right] + \frac{1}{\varepsilon}\left(\hat{b}_\varepsilon [u] + \varepsilon [v]\right) \times \begin{bmatrix} 0 \\ 1 \end{bmatrix} \times H\left[(x - x_{i+1/2}) - (\hat{a} + \varepsilon)(t - t_n)\right] \tag{44}$$

If we calculate the intermediate state, U^*, between the linearized waves 1 and 2, we get:

$$U^* = U^l + \hat{\alpha}_1 \hat{r}_1 = U^r - \hat{\alpha}_2 \hat{r}_2 = \begin{cases} u^r \\ v^l - \frac{\hat{b}_\varepsilon}{\varepsilon}[u] = v^r + \frac{\hat{a}[v] - [g]}{\varepsilon} \end{cases} \tag{45}$$

This is precisely the solution (30) given by the HLLE scheme. Moreover, formula (44) gives the following result:

$$U_\varepsilon(x,t) \underset{\varepsilon \to 0^+}{\to} \begin{cases} u^l + [u] \times H\left[(x - x_{i+1/2}) - \hat{a}(t - t_n)\right] \\ v^l + [v] \times H\left[(x - x_{i+1/2}) - \hat{a}(t - t_n)\right] - \hat{b}(t - t_n)[u] \times \delta\left[(x - x_{i+1/2}) - \hat{a}(t - t_n)\right] \end{cases} \tag{46}$$

where we defined: $\hat{b} \equiv \lim_{\varepsilon \to 0^+} \hat{b}_\varepsilon = ([a(u)v] - \hat{a}[v])/[u]$. Formula (46) is identical to formula (33) when this one is written near $x = x_{i+1/2}$, $t = t_n$. Finally, since $[F_\varepsilon] = \hat{A}_\varepsilon [U]$, we have the following result for $F_\varepsilon(x,t)$:

$$F_\varepsilon(x,t) = F(U^l) + \frac{\hat{a}}{\varepsilon}[u] \times \begin{bmatrix} \varepsilon \\ -\hat{b}_\varepsilon \end{bmatrix} \times H\left[(x - x_{i+1/2}) - \hat{a}(t - t_n)\right] + \frac{(\hat{a} + \varepsilon)}{\varepsilon}\left(\hat{b}_\varepsilon [u] + \varepsilon [v]\right) \times \begin{bmatrix} 0 \\ 1 \end{bmatrix} \times H\left[(x - x_{i+1/2}) - (\hat{a} + \varepsilon)(t - t_n)\right] \tag{47}$$

And, consequently

$$F_{\underset{\varepsilon\to 0^+}{\varepsilon}}(x,t) \to \begin{cases} f(u^l) + \hat{a}[u] \times H\big[(x - x_{i+1/2}) - \hat{a}(t-t_n)\big] \\ g(u^l, v^l) + \hat{a}[v] \times H\big[(x - x_{i+1/2}) - \hat{a}(t-t_n)\big] + \hat{b}[u] \times H\big[(x - x_{i+1/2}) - \hat{a}(t-t_n)\big] \\ \quad -\hat{b}\hat{a}[u](t-t_n) \times \delta\big[(x - x_{i+1/2}) - \hat{a}(t-t_n)\big] \end{cases} \tag{48}$$

This is precisely relation (34) written close to $x = x_{i+1/2}$, $t = t_n$.

Lastly, one can note an interesting result concerning the meaning of the Rankine–Hugoniot deficit, $e(t)$. Indeed, by comparing this quantity with $\dot{b}$, we get the relation:

$$\hat{b}[u] \equiv ([a(u)v] - \hat{a}[v]) \equiv \left.\frac{\mathrm{d}e}{\mathrm{d}t}\right|_{x=\hat{a}t} \tag{49}$$

Consequently, the quantity, $\left.\frac{\mathrm{d}e}{\mathrm{d}t}\right|_{x=\hat{a}t}$, represents the wave strength of the wave that propagates at the velocity $\hat{a}$ and that only brings fluctuations of the linear variable, v. This is precisely the wave that is responsible of the existence of a Dirac measure into the solution of (8).

To conclude, if we select formula (35) to discretize (8) by the HLLE method, in a finite-volume framework, we get the following system of ODEs in time:

$$\left.\frac{\mathrm{d}\overline{U}}{\mathrm{d}t}\right|_i = \frac{F_{i+1/2}(t) - F_{i-1/2}(t)}{\Delta x_i} \tag{50}$$

where we defined: $\overline{U}(t) \equiv \frac{1}{\Delta x_i}\int_{x_{i-1/2}}^{x_{i+1/2}} U(x,t)\mathrm{d}x$.

This system can be integrated by using an explicit Runge–Kutta method. In the numerical experiments that follow, this integration is ensured by the third-order TVD Runge–Kutta scheme [13].

To calculate accurately, $F_{i+1/2}(t)$, we need to evaluate $(u,v)^{l,r}$ at the interface $x = x_{i+1/2}$. This procedure is detailed in the section that follows.

2.3. Hermite-Least-Square-Monotone (HLSM) reconstruction for a weakly hyperbolic system

In [9] we developed a new least-square interpolation that relies upon the cell-averages of the variable and its first spatial derivatives.

By adding a TVD or an ENO constraint into the least-square formulation, we proved that the resulting scheme is fifth-order accurate for smooth data and remains monotone, even in regions where discontinuities may appear.

However, this procedure was only optimized for the non-linear variable, u; no special care was taken to ensure that the linear variable, v, is correctly calculated. This limit becomes detrimental as soon as we intend to capture δ-shock waves.

For this reason, we modify the HLSM reconstruction by adding a new constraint of monotonicity, adapted to the linear variable, v.

In this paper, we only give the modified form of the HLSM interpolation. For a detailed explanation and practical notations concerning this method, we refer the reader to [9].

Initially, the "HLSM-Minmod" reconstruction into the discrete cell $I_i \equiv [x_{i-1/2}, x_{i+1/2}]$, was defined by the following 6×4 algebraic system:

$$\begin{bmatrix} L_{i1} \\ L_{i2} \\ L_{i3} \\ L_{i4} \\ w_i L_{i5} \\ w_i L_{i6} \end{bmatrix} \times \begin{pmatrix} \tilde{a}_1 \\ \tilde{a}_2 \\ \tilde{a}_3 \\ \tilde{a}_4 \end{pmatrix}_i = \begin{pmatrix} \bar{u}_{i-1} - \bar{u}_i \\ \bar{u}_{i+1} - \bar{u} \\ \bar{v}_{i-1} - \bar{v}_i \\ \bar{v}_{i+1} - \bar{v} \\ \widetilde{B}_5 \\ \widetilde{B}_6 \end{pmatrix} \tag{51}$$

where $\{L_{ij}\}_{j\in\{1,..,6\}}$ are vectors with four components that contain metric terms; $\{\tilde{a}_j\}$ are the coefficients of the fourth-degree interpolating polynomial defined into $I_i : \tilde{u}_{\mathrm{opt}}(x) \equiv \sum_{j=0}^{4} \tilde{a}_j (x - x_i)^j$ ($\tilde{a}_0 \equiv \bar{u}_i$) and $\widetilde{B}_{5,6}$ are the monotonicity constraints for the variable u.

If we select a TVD constraint ("HLSM-Minmod" interpolation), we calculate those terms according to the formulae:

$$\begin{cases} \widetilde{B}_5 = -w_i \frac{\Delta x_i}{2} \times \mathrm{minmod}\left(\frac{\bar{u}_{i+1} - \bar{u}_i}{\Delta x_{i+1/2}}, \frac{\bar{u}_i - \bar{u}_{i-1}}{\Delta x_{i-1/2}}\right) \\ \widetilde{B}_6 = -\widetilde{B}_5 \end{cases} \tag{52}$$

w_i is a data-depending weight ensuring that the monotonicity conditions, introduced by $\widetilde{B}_{5,6}$, are activated only in regions of discontinuities.

Practically, w_i is defined as

$$w_i \equiv \alpha \times \frac{IS_i^2}{1+IS_i^2} \tag{53}$$

with: $IS_i \equiv \frac{1}{u_{\max}^2} \times \sum_{k=1}^{4} \Delta x_i^{2k-1} \times \int_{I_i} \left(\frac{d^k \tilde{u}_{\text{opt}}(x)}{dx^k}\right)^2 dx$, is the general indicator of smoothness for the variable, u, over the cell I_i.

α is called the "monotonicity parameter" and is selected to optimize the capture of a possible discontinuity. Practically, this parameter is an O(1) quantity. This way, $w_i \equiv O(\Delta x^4)$ for smooth data while $w_i \equiv O(1)$ at a discontinuity.

Now, if we want to ensure that the linear variable, v, is correctly interpolated without generating non-physical oscillations in regions of singularities, we must introduce two supplementary constraints. To this aim, we just follow the procedure detailed in [9]. Thus, we impose that $\tilde{u}_{\text{opt}}(x)$ is such that

$$\begin{cases} \frac{1}{\Delta x_{i-1/2}} \times \int_{x_{i-1}}^{x_i} \frac{d\tilde{u}_{\text{opt}}}{dx} dx = \bar{v}_i - \frac{\Delta x_i}{2} \times \text{minmod}\left(\frac{\bar{v}_{i+1}-\bar{v}_i}{\Delta x_{i+1/2}}, \frac{\bar{v}_i-\bar{v}_{i-1}}{\Delta x_{i-1/2}}\right) \\ \frac{1}{\Delta x_{i+1/2}} \times \int_{x_i}^{x_{i+1}} \frac{d\tilde{u}_{\text{opt}}}{dx} dx = \bar{v}_i + \frac{\Delta x_i}{2} \times \text{minmod}\left(\frac{\bar{v}_{i+1}-\bar{v}_i}{\Delta x_{i+1/2}}, \frac{\bar{v}_i-\bar{v}_{i-1}}{\Delta x_{i-1/2}}\right) \end{cases} \tag{54}$$

This way, one can generate two supplementary algebraic equations that read as

$$\begin{cases} -\tilde{a}_2 \Delta x_{i-1/2} + \frac{3}{4}\tilde{a}_3 \Delta x_{i-1/2}^2 - \tilde{a}_4 \Delta x_{i-1/2}^3 = -\frac{\Delta x_i}{2} \times \text{minmod}\left(\frac{\bar{v}_{i+1}-\bar{v}_i}{\Delta x_{i+1/2}}, \frac{\bar{v}_i-\bar{v}_{i-1}}{\Delta x_{i-1/2}}\right) \\ \tilde{a}_2 \Delta x_{i-1/2} + \frac{3}{4}\tilde{a}_3 \Delta x_{i-1/2}^2 + \tilde{a}_4 \Delta x_{i-1/2}^3 = \frac{\Delta x_i}{2} \times \text{minmod}\left(\frac{\bar{v}_{i+1}-\bar{v}_i}{\Delta x_{i+1/2}}, \frac{\bar{v}_i-\bar{v}_{i-1}}{\Delta x_{i-1/2}}\right) \end{cases} \tag{55}$$

Or, in a more condensed form:

$$\begin{bmatrix} L_{i7} \\ L_{i8} \end{bmatrix} \times \begin{pmatrix} \tilde{a}_1 \\ \tilde{a}_2 \\ \tilde{a}_3 \\ \tilde{a}_4 \end{pmatrix}_i = \begin{pmatrix} B_7 \\ B_8 \end{pmatrix} \tag{56}$$

with: $\begin{cases} L_{i7,8} \equiv \left[0, \mp\Delta x_{i\mp1/2}, \frac{3}{4}\Delta x_{i\mp1/2}^2, \mp\Delta x_{i\mp1/2}^3\right]^t \\ B_{7,8} \equiv \mp\frac{\Delta x_i}{2} \times \text{minmod}\left(\frac{\bar{v}_{i+1}-\bar{v}_i}{\Delta x_{i+1/2}}, \frac{\bar{v}_i-\bar{v}_{i-1}}{\Delta x_{i-1/2}}\right) \end{cases}$. Adding those constraints to system (51) generates a 8×4 system of which the unknowns are the polynomial coefficients, $\{\tilde{a}_j\}$.

Similarly to the variable u, those constraints must be weighted by a data-depending weight, w_i', specific to the variable v.

To determine this weight, we resort to an accuracy analysis of the resulting scheme. For this purpose, we simplify the problem by considering the discretization of the linear system:

$$U_t + aU_x = 0 \quad (a \equiv Cte > 0) \tag{57}$$

Approximating the spatial operator ($\Delta x_i = \Delta x \equiv Cte$), produces the following result:

$$\frac{U_{i+1/2}^l - U_{i-1/2}^l}{\Delta x} \sim u_x|_i \tag{58}$$

where $U_{i+1/2}^l$ is interpolated from the averaged values $(\bar{u}_i, \bar{v}_i)$ by using the modified HLSM method, typified by (51) and (56).

Influence of the new weight, w_i', is introduced via the modifications:

$$\begin{cases} \widetilde{B}_{7,8} \equiv w_i' \times B_{7,8} \\ L_{i7,8} \to w_i' \times L_{i7,8} \end{cases} \tag{59}$$

Approximation (58) generates an algebraic system for the discrete unknowns $(\bar{u}_i, \bar{v}_i)$. Then, by using the MAPLE symbolic mathematical computer package, we are able to formulate the local truncature error for the spatial operator, according to the values of the weights (w_i, w_i') (see [9] for more technical details concerning this calculation).

We investigate three possibilities for this study.

First, let us consider the case: (a) $\begin{cases} w_i = \alpha \times \Delta x^4 \\ w_i' = \gamma \times \Delta x^4 \end{cases}$.

(α, γ) are supposed to be the "monotonicity parameters" for, respectively, the variables u and $v(\equiv u_x)$. This case corresponds to smooth data for both variables (u, v). Then, the result for the local truncature error, τ_i, gives, for the variable u:

$$\tau_i = \frac{\Delta x^5}{360} \times u_{6x}|_i + O(\Delta x^6) \tag{60}$$

while we obtain, for the variable v:

$$\tau_i = \frac{\Delta x^4}{120} \times u_{6x}|_i + O(\Delta x^5) \tag{61}$$

Therefore, we get the significant result that the values of the monotonicity parameters (α,γ), *have no influence upon the accuracy of the resulting scheme as long as the data remain smooth.*

However, this is no more the case if we select, instead, $w_i' = \gamma \times \Delta x^2$.

Indeed, we then obtain for u:

$$\tau_i = \frac{1}{4}\left(\frac{1}{90} + \frac{11}{20}\gamma^2\right)\Delta x^5 u_{6x}|_i + O(\Delta x^6) \tag{62}$$

and for v:

$$\tau_i = \frac{1}{4}\left(\frac{1}{30} - 3\gamma^2\right)\Delta x^4 \times u_{6x}|_i + O(\Delta x^5) \tag{63}$$

Consequently, w_i' must be at least $O(\Delta x^4)$ in regions of smoothness, in order not to deteriorate the truncature error of the numerical scheme.

Now, let us investigate the case where it exists discontinuities for both variables u and v.

We must have: (b) $\begin{cases} w_i = \alpha \\ w_i' = \gamma \end{cases}$.

In such a case, the minmod function returns the zero value. Consequently, we have: $\widetilde{B}_{5,6,7,8} = 0$. Adding those modified constraints into the algebraic system that discretizes $u_x|_i$, we get for u:

$$\tau_i = \frac{\alpha^2}{2(4+\alpha^2)}\Delta x \times u_{xx}|_i + O(\Delta x^2) \tag{64}$$

and for v:

$$\tau_i = \frac{2}{3}\Delta x \times u_{3x}|_i + O(\Delta x^2) \tag{65}$$

Therefore, we obtain the astonishing result showing that the truncature error does not depend on the parameter γ, if this one remains an O(1)quantity. Both truncature errors are first-order but the parameter α only appears to weight the dissipative terms of the numerical scheme.

Lastly, we study the following case: (c) $\begin{cases} w_i = \alpha \times \Delta x^4 \\ w_i' = \gamma \end{cases}$.

This case aims at taking into account data for which u remains smooth while v may present singularities: this is the case of a contact discontinuity for the variable, v, for example.

We must have: $\widetilde{B}_{7,8} = 0$.

Then, we get for u:

$$\tau_i = \frac{3}{25}\Delta x^2 \times u_{3x}|_i + O(\Delta x^3) \tag{66}$$

and for v:

$$\tau_i = \frac{13}{5}\Delta x \times u_{3x}|_i + O(\Delta x^2) \tag{67}$$

Therefore, although w_i is an $O(\Delta x^4)$ quantity, the resulting scheme is second-order for the variable u and first-order for v. Once again, those results are free of the value of the monotonicity parameter γ.

To conclude this analysis, we can say that the value of the parameter γ has no importance as long as this one remains an O(1) quantity. Practically, α is the only parameter that makes it possible to weight the dissipative nature of the numerical scheme.

This result is advantageous since it does not lessen the robustness of the HLSM method, initially developed in [9].

Using those results, we suggest the following definition for the new weight, w_i':

$$w_i' \equiv \frac{IS_i'}{1 + IS_i'} \tag{68}$$

with: $IS_i' \equiv \frac{1}{u_{\max}^2} \times \sum_{k=2}^{4} \Delta x_i^{2k-1} \times \int_{I_i} \left(\frac{d^k \tilde{u}_{opt}(x)}{dx^k}\right)^2 dx$, the general smoothness indicator for the variable, v.

This way, according to the definition of IS_i', $w_i' = O(\Delta x^4)$, for smooth data in v, while $w_i' = O(1)$ when v presents a singularity.

Summarizing, the modified version of the HLSM method is constituted by formulae (51)–(53), (56), (59) and (68). When $w_i' \equiv 0$, the method coincides with the HLSM method initially developed in [9].

Now, to check the monotone behaviour of the resulting scheme and its convergence properties, we present numerical experiments in the section that follows.

2.4. Numerical experiments: the Burgers equation

We consider the discretization of system (8) for the choice: $f(u) \equiv u^2/2$. The result is the extended version of the scalar Burgers equation. The discretization is ensured by combining the HLLE method, typified by formula (35), and the modified HLSM reconstruction: the resulting scheme will be called the "Hermite-HLLE" scheme, in what follows.

Unless mentioned, the mesh is supposed to be uniform and N grid points are used to discretize the problem. The *CFL* number is defined as $\max_i |u_i^n| \Delta t/\Delta x$ and its value is taken to 0.5, except for the accuracy tests where we selected $\Delta t = O(\Delta x^2)$.

For those experiments, the parameter α is set to the value 6, which is the value optimized by trials and errors, when discontinuities appear into the solution.

Lastly, to compare the HLSM reconstruction with a more "classical" interpolation procedure, we added the HUWENO5 scheme of Qiu and Shu, [20], as a reference.

To begin, system (8) is solved for the initial conditions: $U_0(x) = \begin{cases} 1/2 + \sin(\pi x) \\ \pi \cos(\pi x) \end{cases} \quad \forall x \in [0,2]$, and a 2-periodic boundary condition.

When $t = 1/2\pi$, the solution is still smooth and the discrete errors (L_1 and L_∞ norms) and numerical orders of accuracy are shown in Table 1 (variable u) and Table 2 (variable $v \equiv u_x$). As one can note it, the scheme reaches its designed order of accuracy for both variables u and v.

When $t = 3/2\pi$, a shock has already appeared in the solution and it is located at $x_s = 1.238$.

Fig. 2(a) and (b) display the numerical solution for both variables u and v, on a uniform mesh with $N = 80$ grid points. As one can see it, Fig. 2(a), the shock is captured without any numerical oscillation. Moreover, considering Fig. 2(b), this shock is a δ-shock wave since it appears as a singularity for the solution, v. We can see that this singularity is captured without spurious oscillations. When the mesh is refined, this solution converges towards a Dirac solution, for the variable v.

Next, Fig. 2(c) shows the numerical solution on a stretched mesh ($\Delta x_{\min}/\Delta x_{\max} = 0.10$) near the shock place: the shock keeps being captured without any numerical oscillations. Lastly, Fig. 2(d) shows the evolution of the weights w_i and w_i' in the computation domain: only four values are O(1), for each weight. It is at these points that the monotonicity constraints play a role. For this test, the HUWENO5 scheme [20], gives very similar results, both for the variable and its first derivative, Fig. 3.

To assess the local behaviour of the monotonicity constraints, we list the discretization errors at a distance 0.05 away from the shock ($|x - x_s| \geqslant 0.05$). Tables 3 and 4 present those results for, respectively, the variables u and v. As can be seen, the orders of magnitude of the errors are not very far from the continuous case. Concerning the HUWENO5 scheme, numerical results are given in Tables 5 and 6: as one can observe it, there is an inconsistency in the computation of the first derivative since numerical results diverge, when the mesh is refined; however, this result does not deteriorate the non-oscillatory behaviour of the WENO procedure, Fig. 3(a) the fact that the first derivative is multiplied by an $O(\Delta x)$ term in the reconstruction procedure, lessens the influence of this inconsistency – at least on coarse meshes where the singularity into the first derivative is interpreted as continuous by the numerical scheme. When the mesh is sufficiently dense, the singularity begins to appear into the numerical solution, v. Table 5 shows us that this singularity has a detrimental influence on the convergence rate of the numerical solution, u, although this problem is not visually detected if one looks at the profiles of the solution, Fig. 3(a).

Table 1
Burgers equation: continuous case

N	L_1 error	L_1 order	L_∞ error	L_∞ order
10	1.36×10^{-2}	–	2.56×10^{-2}	–
20	5.01×10^{-4}	4.8	2.32×10^{-3}	3.1
40	8.05×10^{-6}	5.9	4.18×10^{-5}	5.8
80	2.52×10^{-7}	5	1.95×10^{-6}	5
160	8.27×10^{-9}	5	6.35×10^{-8}	5

$u_t + uu_x = 0$; $u(x, t = 0) = 1/2 + \sin(\pi \times x)$; Hermite-HLLE scheme ($\alpha = 6$) with periodic boundary conditions; $t = 1/2\pi$;$\Delta t = \Delta x^2/2$;L_1 and L_∞ errors for $u(x)$.

Table 2
Burgers equation: continuous case

N	L_1 error	L_1 order	L_∞ error	L_∞ order
10	5.0×10^{-2}	–	0.12	–
20	2.28×10^{-2}	2.1	1.85×10^{-1}	0.6
40	2.56×10^{-3}	3.2	2.61×10^{-2}	2.8
80	1.76×10^{-4}	3.8	2.54×10^{-3}	3.1
160	1.17×10^{-5}	4	1.72×10^{-4}	3.9
320	7.32×10^{-7}	4	1.12×10^{-5}	4

$u_t + uu_x = 0$; $u(x, t = 0) = 1/2 + \sin(\pi \times x)$; Hermite-HLLE scheme ($\alpha = 6$) with periodic boundary conditions; $t = 1/2\pi$; $\Delta t = \Delta x^2/2$; L_1 and L_∞ errors for $u_x(x)$.

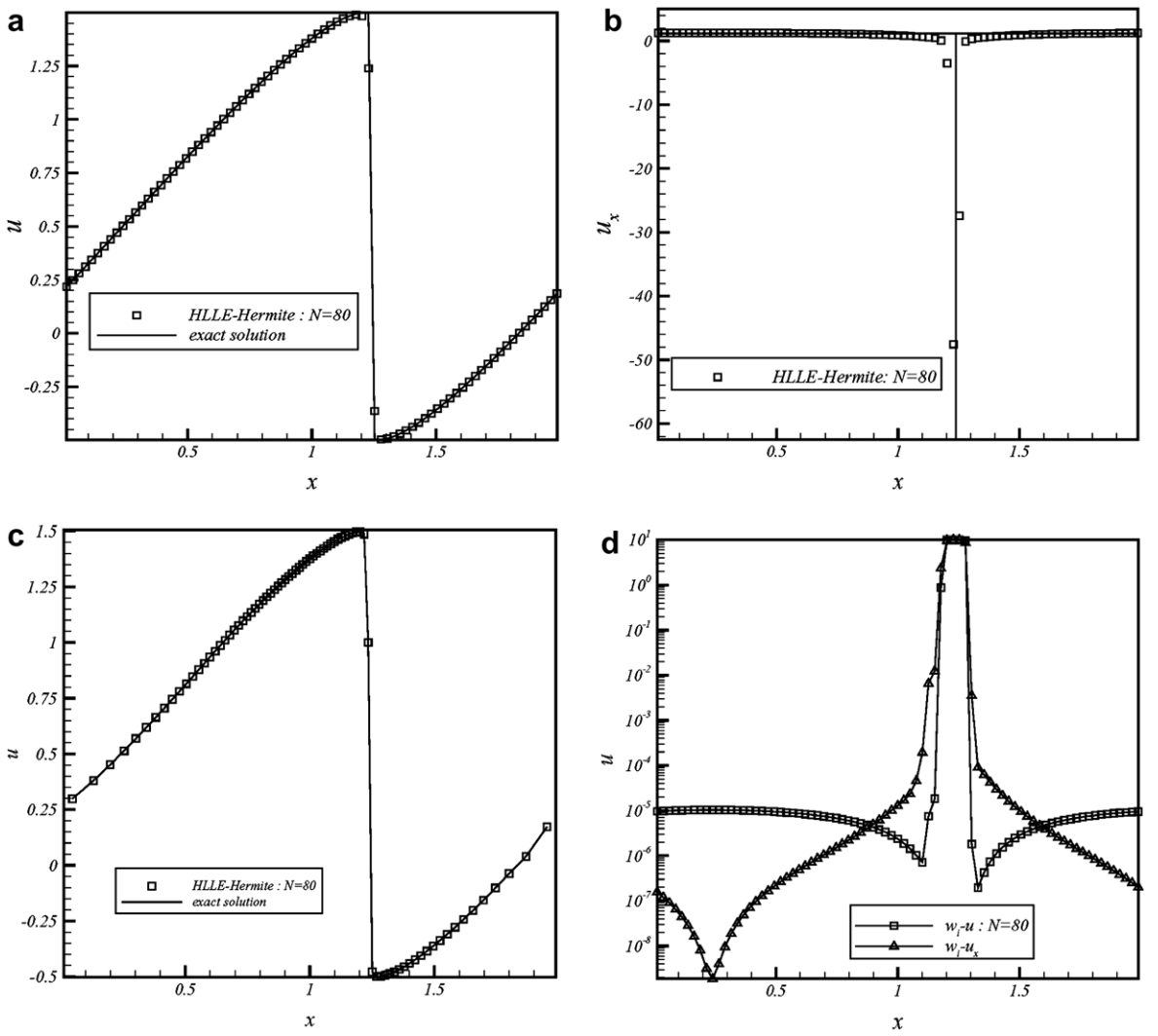

Fig. 2. Burgers equation. $u(x,\ t=0)=1/2+\sin(\pi x)$, $t=3/2\pi$, $N=80$, CFL = 0.5. Hermite-HLLE scheme: (a) uniform mesh, (b) first derivative u_x, (c) non-uniform mesh ($\Delta x_{\min}/\Delta x_{\max}=0.10$) and (d) non-linear weights.

Now, we use the mathematical results given in [6] as test-cases for our computations. Those test-cases are Riemann problems and include all the possible solutions for a scalar problem.

The first test-case we consider for system (8), is given by the initial data below:

$$U_0(x)=\begin{cases}(-2,1) & x\leqslant 1\\ (4,-2) & x>1\end{cases}$$

This is the case for which: $u^l < u^r$.

The exact solution is expressed as

$$U(x,t)=\begin{cases}(-2,1) & x<-2t\\ (x/t,0) & -2t\leqslant x\leqslant t\\ (4,-2) & x>t\end{cases}$$

This solution includes two contact discontinuities and the vacuum, for the variable v.

Fig. 4 present the numerical results obtained at $t=1/8$ and for $N=80$. As one can see it, the rarefaction wave, which exists for the variable u, is correctly approximated, Fig. 4(a). Similarly, the solution for v exhibits the presence of the vacuum zone and the contact discontinuities, Fig. 4(b); no numerical oscillations appear into the solution. However, those discontinuities are somewhat dissipated. Moreover, one can note the appearance of a discontinuity in the profile of v, for the vacuum zone: at this place, the second derivative of the numerical solution becomes discontinuous. This behaviour results in an $O(\Delta x)$ error for the variable, v.

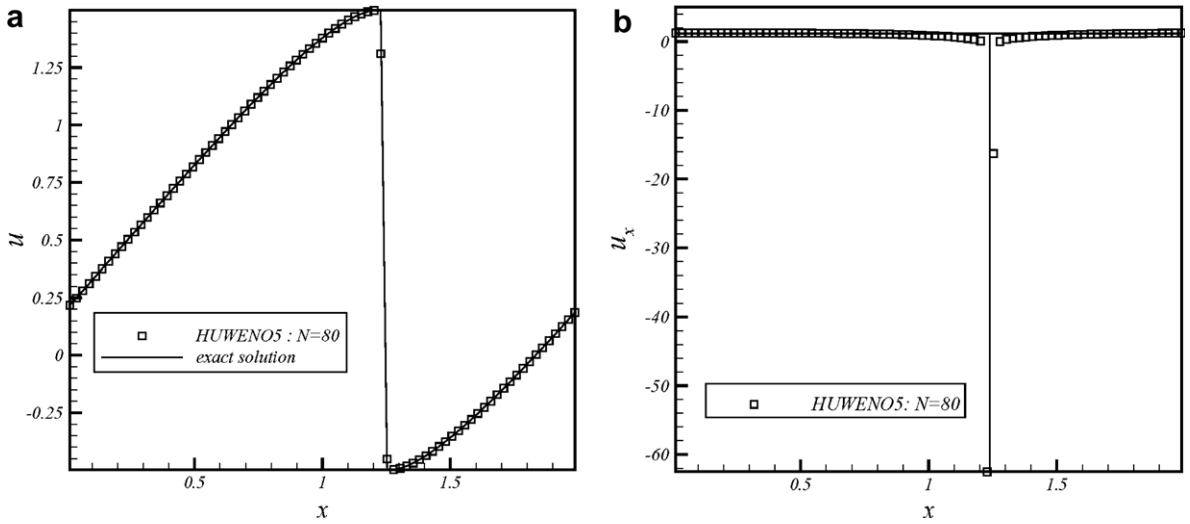

Fig. 3. Burgers equation. $u(x, t = 0) = 1/2 + \sin(\pi x)$, $t = 3/2\pi$, $N = 80$, CFL = 0.5. HUWENO5 scheme [20]: (a) $u(x)$ uniform mesh and (b) first derivative.

Table 3
Burgers equation: discontinuous case

N	L_1 error	L_1 order	L_∞ error	L_∞ order
10	2.50×10^{-2}	–	7.20×10^{-2}	–
20	4.0×10^{-3}	2.6	3.85×10^{-2}	0.9
40	4.91×10^{-4}	3	1.18×10^{-2}	1.7
80	5.38×10^{-5}	3.2	3.33×10^{-3}	1.8
160	3.96×10^{-6}	3.8	4.89×10^{-4}	2.8
320	2.06×10^{-8}	7.6	4.74×10^{-6}	6.6

$u_t + uu_x = 0$; $u(x, t = 0) = 1/2 + \sin(\pi \times x)$; $|x - x_s| \geqslant 0.05$ Hermite-HLLE scheme ($\alpha = 6$) scheme with periodic boundary conditions; $t = 3/2\pi$; $\Delta t = \Delta x^2/2$; L_1 and L_∞ errors for $u(x)$.

Table 4
Burgers equation: discontinuous case

N	L_1 error	L_1 order	L_∞ error	L_∞ order
80	4.26×10^{-3}	–	2.60×10^{-1}	–
160	3.90×10^{-4}	3.1	3.49×10^{-2}	2.9
320	5.43×10^{-6}	6.2	6.81×10^{-4}	5.9

$u_t + uu_x = 0$; $u(x, t = 0) = 1/2 + \sin(\pi \times x)$; $|x - x_s| \geqslant 0.05$ Hermite-HLLE scheme ($\alpha = 6$) scheme with periodic boundary conditions; $t = 3/2\pi$; $\Delta t = \Delta x^2/2$; L_1 and L_∞ errors for $u_x(x)$.

Table 5
Burgers equation: discontinuous case

N	L_1 error	L_1 order	L_∞ error	L_∞ order
10	1.40×10^{-2}	–	7.81×10^{-2}	–
20	5.07×10^{-4}	4.8	2.06×10^{-3}	5.2
40	3.024×10^{-4}	–	4.39×10^{-3}	–
80	3.00×10^{-5}	3.3	6.75×10^{-4}	2.8
160	1.80×10^{-5}	–	6.58×10^{-4}	–
320	1.51×10^{-5}	–	2.84×10^{-4}	–

$u_t + uu_x = 0$; $u(x, t = 0) = 1/2 + \sin(\pi \times x)$; $|x - x_s| \geqslant 0.05$ HUWENO5 scheme [20], with periodic boundary conditions. $t = 3/2\pi$; $\Delta t = \Delta x^2/2$; L_1 and L_∞ errors for $u(x)$.

To check this, we present numerical results for $N = 160$, Fig. 4(c). One can note that this discontinuity is attenuated; furthermore, the contact discontinuities are less dissipated: the HLLE-Hermite scheme seems to converge to entropy correct solution, for this case.

Table 6
Burgers equation: discontinuous case

N	L_1 error	L_1 order	L_∞ error	L_∞ order
80	5.60×10^{-3}	–	1.44×10^{-1}	–
160	7.90×10^{-3}	–	2.45×10^{-1}	–
320	1.50×10^{-2}	–	3.30×10^{-1}	–

$u_t + uu_x = 0$; $u(x,\ t=0) = 1/2 + \sin(\pi \times x)$; $|x - x_s| \geqslant 0.05$ HUWENO5 scheme [20], with periodic boundary conditions. $t = 3/2\pi$; $\Delta t = \Delta x^2/2$; L_1 and L_∞ errors for $u_x(x)$.

Fig. 5 present numerical results obtained with the HUWENO5 scheme. As one can see it, the rarefaction wave is correctly calculated almost everywhere, except at the top point of the u-profile, Fig. 5(a): there is a maximum that does not exist when the HLSM reconstruction is used, Fig. 4(a). This behaviour can be explained if one considers Fig. 5(b): the numerical solution is highly oscillatory and the discontinuities in v ($\equiv u_x$) are not correctly captured.

When the mesh is refined, those results are not improved, Fig. 5(c) and (d). Indeed, the amplitude of the oscillations in v increases with the mesh resolution and tends to compensating for the reduction of the size mesh, Δx, so that the peak in the top of the u-profile remains visible, Fig. 5(c).

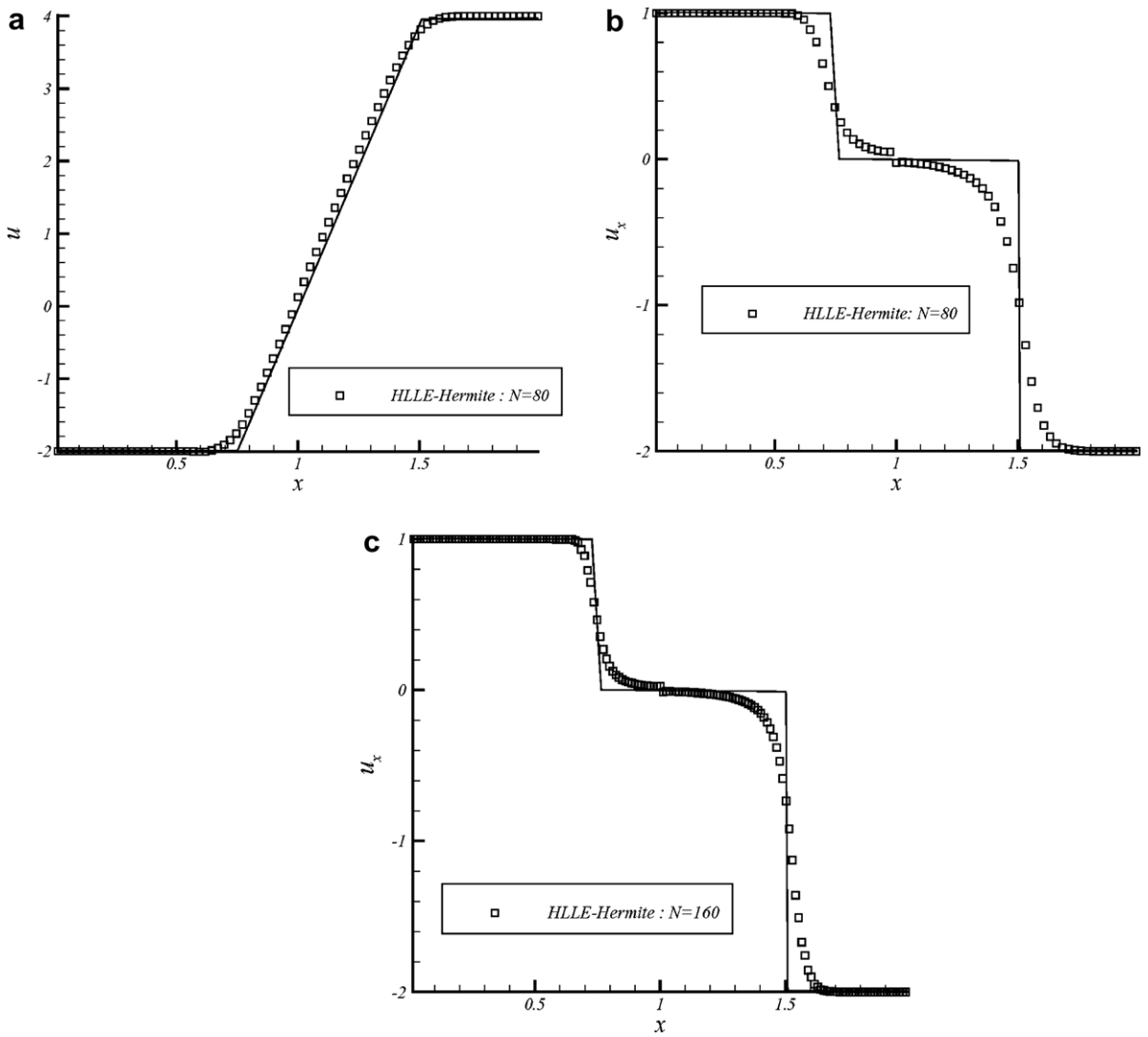

Fig. 4. Burgers equation. $(u,\ u_x)^l|_{t=0} = (-2,1)$ if $x < 1$; $(u,\ u_x)^r|_{t=0} = (4,-2)$ if $x > 1$. $t = 1/8$, $CFL = 0.5$. Hermite-HLLE scheme: (a) $u(x)$ for $N = 80$, (b) $u_x(x)$ for $N = 80$ and (c) $u_x(x)$ for $N = 160$.

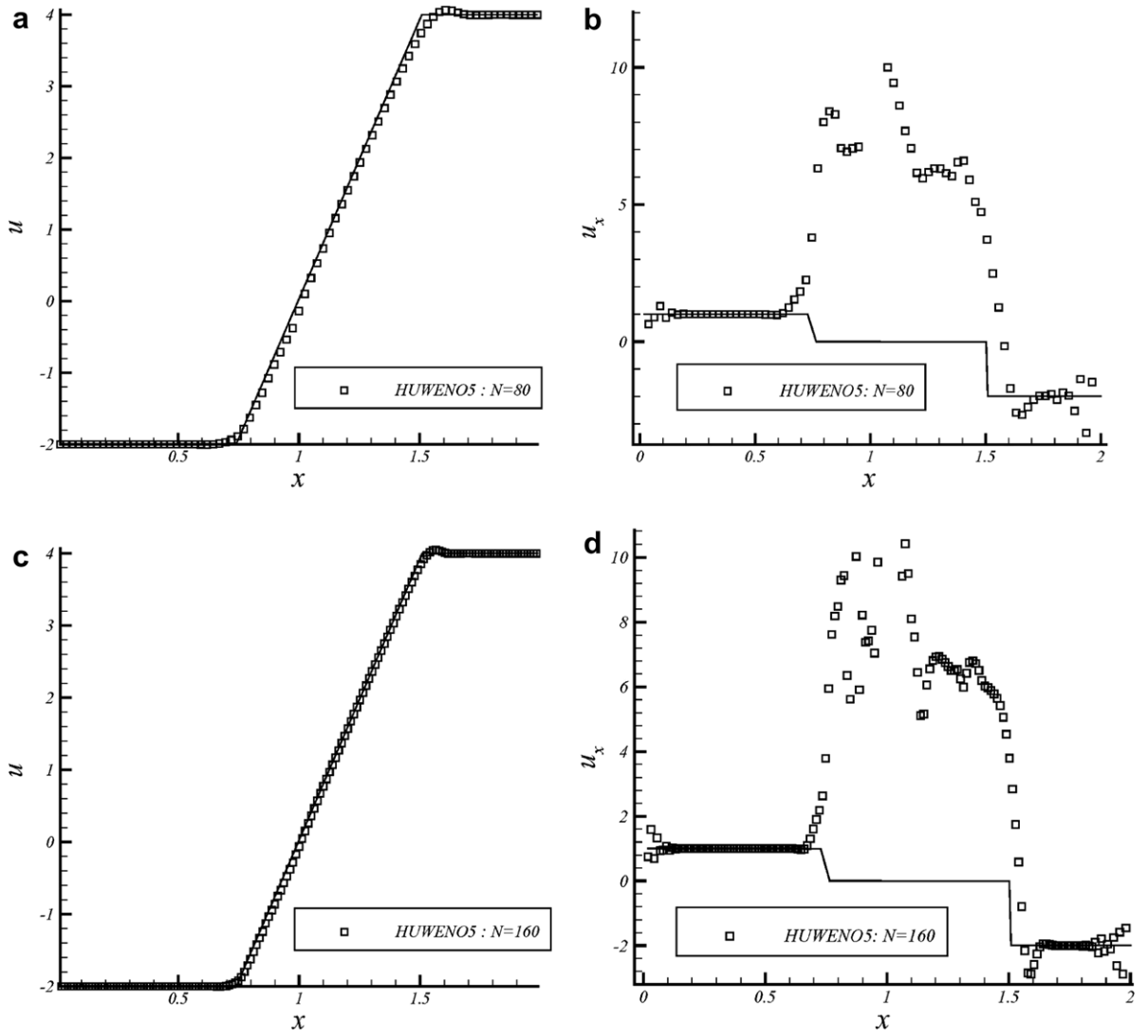

Fig. 5. Burgers equation. $(u, u_x)^l|_{t=0} = (-2,1)$ if $x < 1$;$(u, u_x)^r|_{t=0} = (4, -2)$ if $x > 1$. $t = 1/8$, CFL = 0.5. HUWENO5 scheme [20]: (a) $u(x)$for $N = 80$, (b) $u_x(x)$ for $N = 80$, (c) $u(x)$ for $N = 160$ and (d) $u_x(x)$ for $N = 160$.

Now, let us consider the following test-case:

$$U_0(x) = \begin{cases} (-2,1) & x < 1 \\ (-4,-50) & x = 1 \\ (4,-2) & x > 1 \end{cases}$$

According to [6], the exact solution to this problem is given by

$$U(x,t) = \begin{cases} (-2,1) & x < x(t) \\ (u_\delta(t), w(t) \times \delta(x - x(t))) & x = x(t) \\ (u(x/t), 0) & x(t) < x < 4t \\ (4,-2) & x \geqslant 4t \end{cases}$$

where $(u_\delta(t), w(t), x(t))$ is solution of the system:

$$\begin{cases} \frac{dx}{dt} = u_\delta \\ \frac{dw}{dt} = -[v]u_\delta + [vu] \\ \frac{dwu_\delta}{dt} = -[vu] \times u_\delta + [vu^2] \end{cases}$$

with the initial conditions: $x(0) = 1$, $w(0) = -50$, $u_\delta = -4$ and $[v] = -3$, $[vu] = -6$, $[vu^2] = -28$.

This solution contains two contact discontinuities, a vacuum zone and a δ-shock wave.

Fig. 6 present numerical results for this case. The computations are run up to $t = 0.10$. For $N = 160$, we can see that the numerical solution is still under solved. This is true not only for the variable, v, Fig. 6(b), but also for the variable u. Once again, the discontinuity of the second derivative in the vacuum region introduces a jump into the v profile. If we increase the resolution ($N = 320$), results are improved, Fig. 6(c) and (d), and the convergence to the entropy solution seems to be correct.

Numerical results obtained with the HUWENO5 scheme still show large oscillations for the variable, v, Fig. 7(b); as one can note it, those oscillations create non-physical extrema into the solution for u, at the top and the bottom of the rarefaction wave, Fig. 7(a).

The ultimate test we consider is typified by the following initial conditions:

$$U_0(x) = \begin{cases} (-2, 1) & x < 1 \\ (2, -50) & x = 1 \\ (4, -2) & x > 1 \end{cases}$$

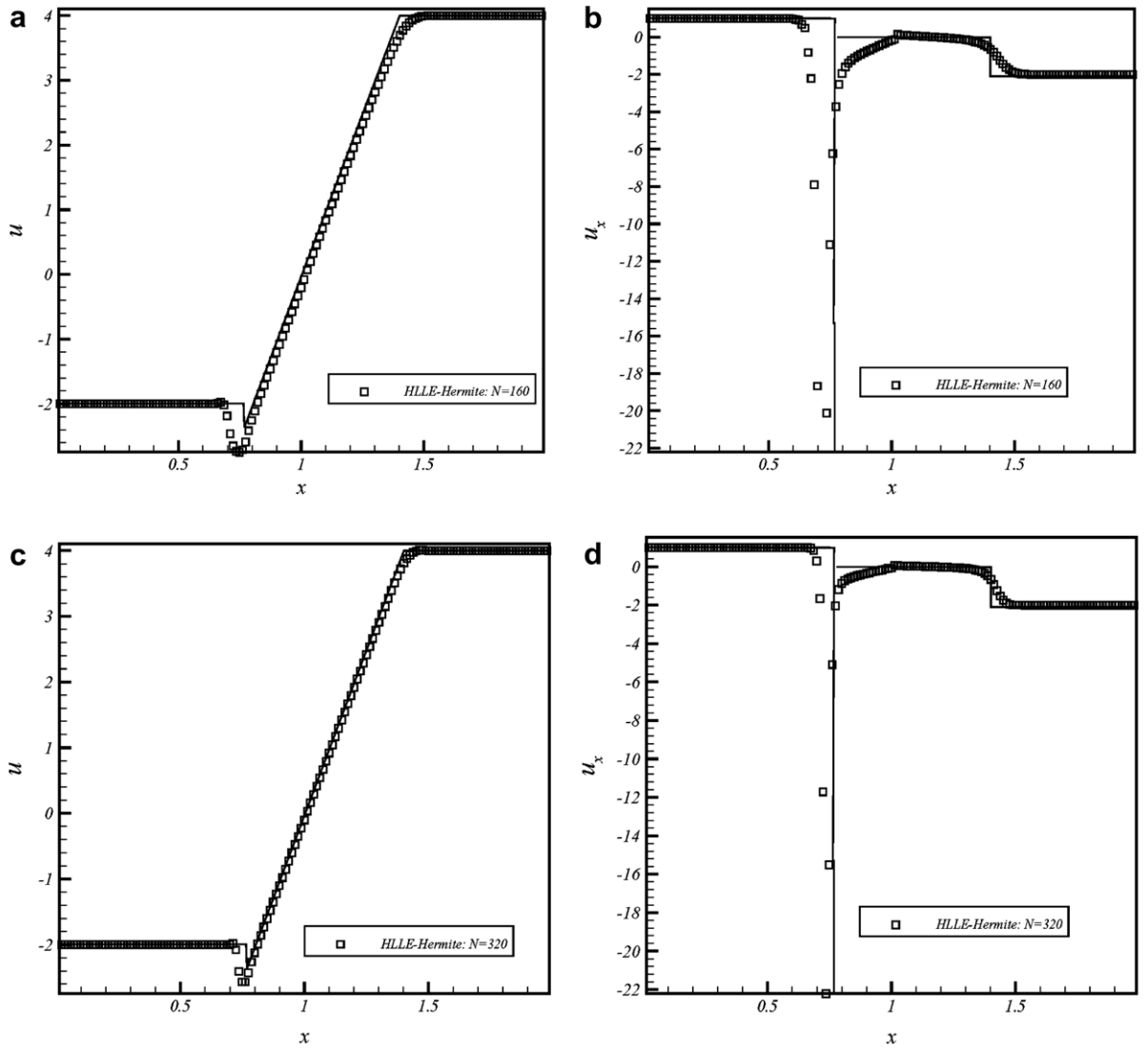

Fig. 6. Burgers equation. $(u, u_x)^l|_{t=0} = (-2,1)$ if $x < 1$; $(u, u_x)^r|_{t=0} = (4, -2)$ if $x > 1$;$(u, u_x)^l|_{t=0} = (-4, -50)$ if $x = 1$. $t = 1/10$, CFL = 0.5. Hermite-HLLE scheme: (a) $u(x)$ for $N = 160$, (b) $u_x(x)$ for $N = 160$, (c) $u(x)$ for $N = 320$ and (d) $u_x(x)$ for $N = 320$.

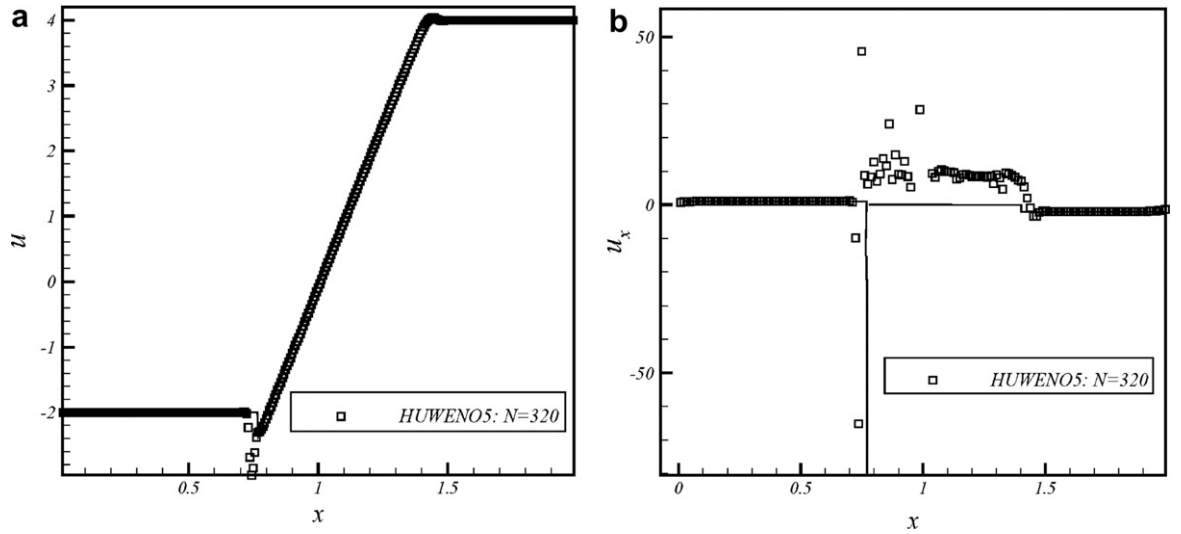

Fig. 7. Burgers equation. $(u, u_x)^l|_{t=0} = (-2,1)$ if $x < 1$; $(u, u_x)^r|_{t=0} = (4, -2)$ if $x > 1$; $(u, u_x)^l|_{t=0} = (-4, -50)$ if $x = 1$. $t = 1/10$, CFL = 0.5. HUWENO5 scheme [20]: (a) $u(x)$ for $N = 320$ and (b) $u_x(x)$ for $N = 320$.

The exact solution is given by

$$U(x,t) = \begin{cases} (-2,1) & x \leqslant -2t \\ (u(x/t),0) & -2t < x < 2t \\ (2,-50 \times \delta(x-2t)) & x = 2t \\ (u(x/t),0) & 2t < x < 4t \\ (4,-2) & x \geqslant 4t \end{cases}$$

This solution is very demanding for a numerical scheme, especially concerning the linear variable, v. It contains two contact discontinuities, two vacuum zones and a δ-shock wave. Fig. 8 present numerical results at $t = 0.10$. For $N = 160$, we can see that the exact solution, for u, is correctly approximated by the scheme, Fig. 8(a).

This is no more the case for the variable, v. Indeed, for $N = 640$, the solution is too much dissipated, Fig. 8(b): this is especially true for the second contact discontinuity situated at $x = 1.40$.

When we increase N ($N = 1280$), the contact discontinuities are better predicted, Fig. 8(c); however, the capture of the δ-shock is deteriorated.

Therefore, this test-case shows the limits of the scheme: for a complex linear solution of a weakly hyperbolic system, fifth-order accuracy is far from to be sufficient. However, one must note two points to attenuate this result: firstly, if we are only interested by the non-linear variable, u, results are good (see Fig. 8(a)); secondly, even if the linear variable is under predicted, this one apparently converges to the correct entropy solution when the mesh is refined.

Lastly, Fig. 9 display numerical results obtained with the HUWENO5 scheme. As expected, the singularities in the linear variable, v, are not at all captured, Fig. 9(b); even if the consequence of this failure is largely attenuated for the variable u, Fig. 9(a), one can notice overshoots at the discontinuity points of the variable v, while the rarefaction wave is slightly distorted when compared with the exact solution, Fig. 9(a).

To conclude, those experiments validate the preceding theoretical study: δ-shock waves are correctly captured by the Hermite-HLLE scheme. The new constraints added to the initial HLSM method, prevent any non-physical oscillation in the linear variable. Moreover, comparing with a more classical WENO procedure, it appears that those oscillations, if unlimited, can have a detrimental influence on the behaviour of the non-linear variable: although attenuated by an $O(\Delta x)$ term, those oscillations become larger when the mesh is refined, leading to overshoots and reducing the convergence rate for the non-linear variable.

In addition, the HLLE scheme gives the correct propagation speed for a singular or a regular discontinuity.

The procedure being validated, it is left to extending it to a non-linear hyperbolic system of conservation laws, namely the one-dimensional Euler equations for gas dynamics.

3. HLL Riemann solver for weakly hyperbolic systems: the 1D Euler equations

3.1. Notations

We consider the one-dimensional Euler equations in the following conservative form:

$$\frac{\partial \mathbf{U}}{\partial t} + \frac{\partial f(U)}{\partial x} = 0 \tag{69}$$

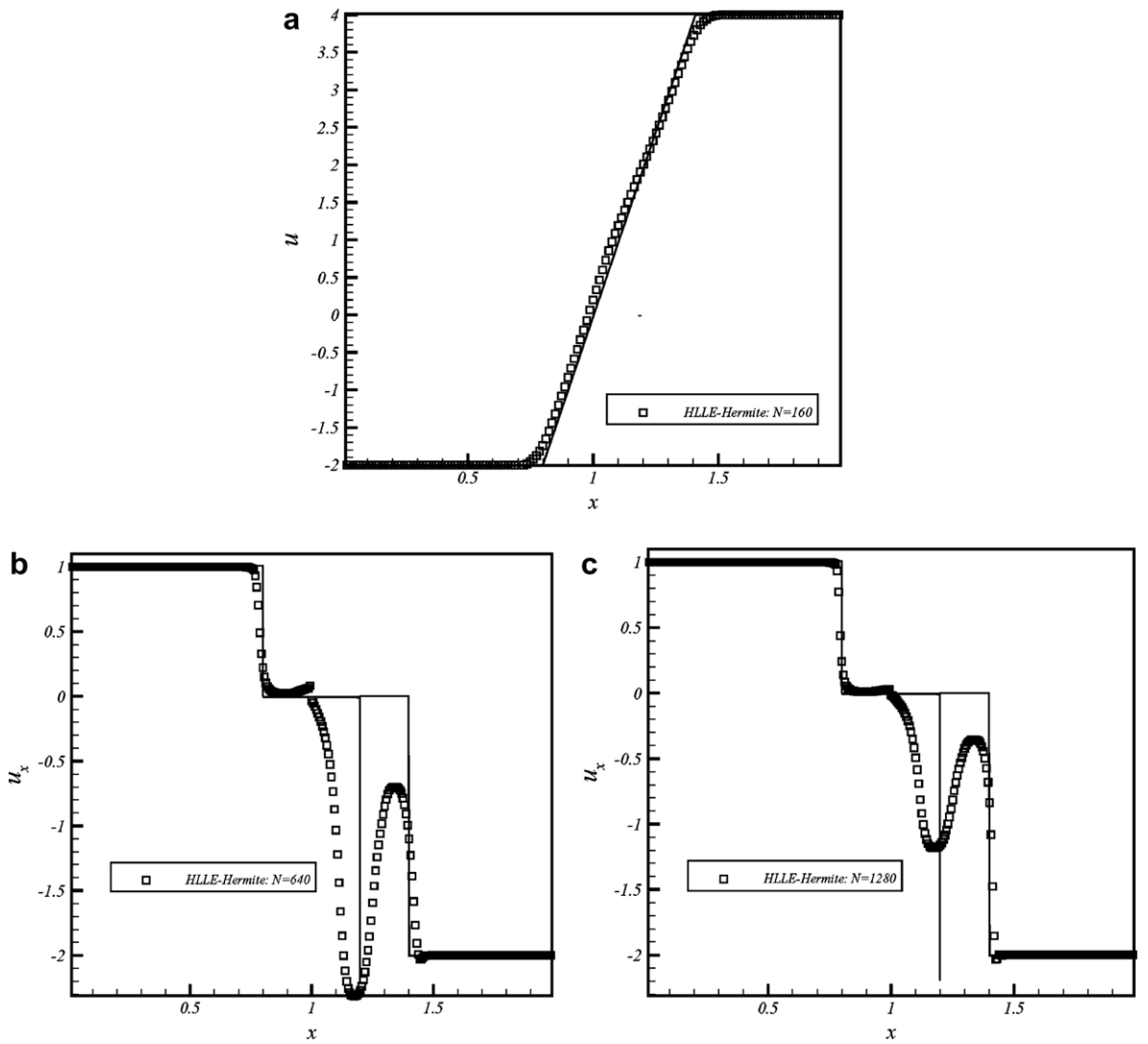

Fig. 8. Burgers equation. $(u, u_x)^l|_{t=0} = (-2,1)$ if $x < 1$; $(u, u_x)^r|_{t=0} = (4, -2)$ if $x > 1$; $(u, u_x)^l|_{t=0} = (2, -50)$ if $x = 1$. $t = 1/10$, CFL = 0.5. Hermite-HLLE scheme: (a) $u(x)$ for $N = 160$, (b) $u_x(x)$ for $N = 640$ and (c) $u_x(x)$ for $N = 1280$.

where: $\mathbf{U} \equiv [\rho, \rho u, e]^t$, $\mathbf{F} \equiv [\rho u, \rho u^2 + p, \rho u H]^t$

$H \equiv (e + p)/\rho$ is the specific total enthalpy and this set of equations is closed by the equation-of- state of an ideal gas: $p = (\gamma - 1)(e - \rho u^2/2)$, $\gamma = 1.40$.

By deriving (69) with respect to x, we get the following set of systems:

$$\begin{cases} \frac{\partial \mathbf{U}}{\partial t} + \frac{\partial f(U)}{\partial x} = 0 \\ \frac{\partial \mathbf{V}}{\partial t} + \frac{\partial g(U,V)}{\partial x} = 0 \end{cases} \tag{70}$$

where we defined: $\mathbf{V} \equiv [(\rho)_x, (\rho u)_x, e_x]^t$, $g \equiv [(\rho u)_x, (\rho u^2 + p)_x, (\rho u H)_x]^t$.

Defining the Jacobian matrix, $A \equiv \partial f / \partial U$, we get the following property for the flux g: $g \equiv f_x = A(U) \times V$.

This system constitutes the extended form of the 1D Euler equations. In a more condensed form, (70) can be equivalently written as

$$\begin{cases} \widetilde{U}_t + F(\widetilde{U})_x = 0 \\ \widetilde{U} \equiv [U, V]^t; F \equiv [f, g]^t \end{cases} \tag{71}$$

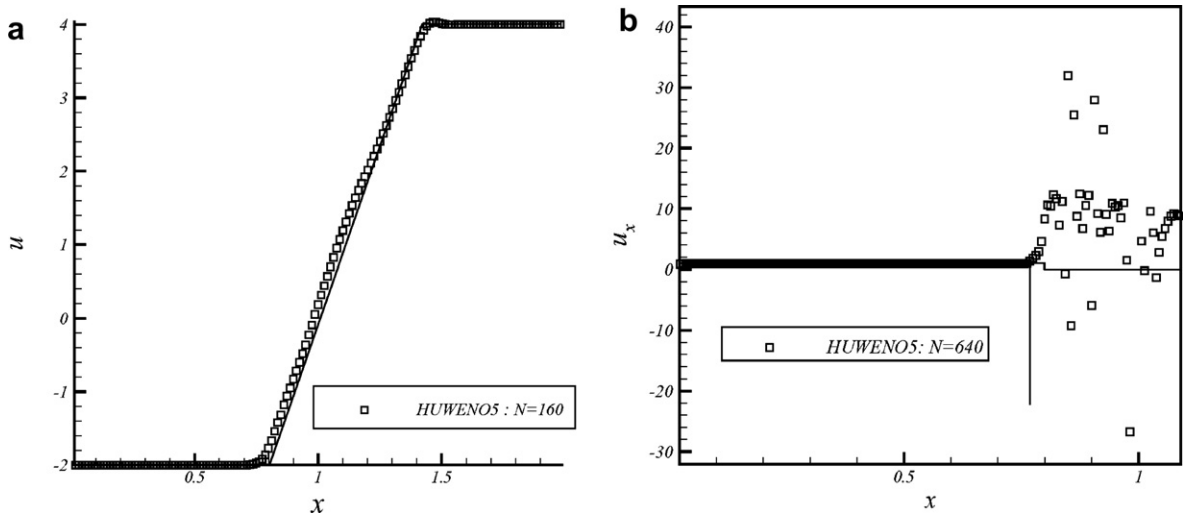

Fig. 9. Burgers equation. $(u, u_x)^l|_{t=0} = (-2,1)$ if $x < 1$; $(u, u_x)^r|_{t=0} = (4, -2)$ if $x > 1$; $(u, u_x)^l|_{t=0} = (2, -50)$ if $x = 1$. $t = 1/10$, CFL = 0.5. HUWENO5 scheme: (a) $u(x)$ for $N = 160$ and (b) $u_x(x)$ for $N = 640$.

In what follows, we shall necessitate the convective form of the extended Euler equations. This form reads as

$$\begin{cases} \widetilde{U}_t + \mathcal{A}(\widetilde{U})_x = 0 \\ \mathcal{A}(\widetilde{U}) \equiv \frac{\partial F}{\partial U} = \begin{bmatrix} A(U) & 0 \\ B(U,V) & A(U) \end{bmatrix} \end{cases} \tag{72}$$

with: $B(U, V) \equiv \partial g/\partial U$.

The eigenvalues of $\mathcal{A}$ are the eigenvalues of $A(U)$; therefore, system (72) or (71) is weakly hyperbolic.

To be able to calculate possible δ-shock waves into the solution of (72) or (71), we need to discriminate between a contact discontinuity and a shock wave. For this reason, we adapt the so-called "HLLC Riemann solver", devised in [15,16], to our problem: this scheme will be named in what follows, the "Hermite-HLLC" scheme.

3.2. A HLLC Riemann solver for the extended Euler equations

The henceforth-classical HLLE Riemann solver has many advantages: it automatically satisfies an entropy condition, captures isolated shocks and preserves positivity [10]. However, it is unable to exactly capture isolated contact discontinuities.

The HLLC Riemann solver, initially elaborated by Toro et al [14], suppresses this drawback. It is a two-state HLL approximation that introduces the contribution of a contact discontinuity.

The solution we propose is an extended version of the HLLC scheme for weakly hyperbolic systems of conservation laws.

Unfortunately, the equivalent of theoretical results we used in the scalar case does not exist yet for the 1D Euler equations. Consequently, we can only use a heuristic analogy with the scalar results, in order to develop the Hermite-HLLC scheme. In that sense, the calculations that follow contain a certain degree of arbitrariness.

To begin, consider two averaged intermediate states, $\widetilde{U}_l^*$ and $\widetilde{U}_r^*$, separated by a contact discontinuity, of which speed is denoted by λ^m.

Defining this contact wave, we have the first relations for the variable U:

$$\lambda^m \equiv u^m = u_l^* = u_r^* \tag{73.a}$$

Then, using the Rankine–Hugoniot conditions for U, we deduce that

$$p_l^* = p_r^* \equiv p^m \tag{73.b}$$

Relations (73.a) and (73.b) entirely define the contact discontinuity, for the variable U.

Now, let us calculate the relations verified by the variable V, for this same discontinuity. To do those calculations, we made the significant assumption that *the contact discontinuity in U generates also a discontinuity in V that propagates at the same velocity*. Therefore, according to the scalar results, there are no reasons for a Rankine–Hugoniot deficit to exist for this discontinuity. Thus, we conclude that such a discontinuity in V is bounded and cannot be identified with a δ-shock wave: for this reason, we decided to call this discontinuity in V, a contact discontinuity. In the absence of theoretical results concerning this problem, this choice aims at being an equivalent of solution typified by Eqs. (16) and (17), in the scalar case.

Then, the Rankine–Hugoniot relations verified by the variable V, for a discontinuity propagating at the velocity, u^m, are as follows (the "*" are temporarily omitted, for simplicity):

$$\begin{cases} (\rho u)_x^l - (\rho u)_x^r = u^m(\rho_x^l - \rho_x^r) \\ (\rho u^2 + p)_x^l - (\rho u^2 + p)_x^r = u^m((\rho u)_x^l - (\rho u)_x^r) \\ \{u(e+p)\}_x^l - \{u(e+p)\}_x^r = u^m(e_x^l - e_x^r) \end{cases} \tag{74}$$

Using (73.a) into the first equation of (74), gives the first result verified across the contact wave in V:

$$[\rho u_x] = 0 \tag{75.a}$$

Then, using this result with (73.a) and (73.b) into the second equation of (74), we get the second useful relation:

$$[p_x] = 0 \tag{75.b}$$

Finally inserting those results into the last equation of (74), this equation is identically verified.

Therefore, the contact discontinuity that propagates at the speed u^m, is typified by the following relations across this wave:

$$\begin{cases} [u] = [p] = 0 \\ [\rho u_x] = [p_x] = 0 \end{cases} \tag{76}$$

Now, we are able to completely calculate the intermediate states, $\widetilde{U}_l^*$ and $\widetilde{U}_r^*$, by using those results.

Firstly, we calculate the intermediate states for the vectors U_l^* and U_r^*: this calculation is detailed in [14,16] and will not be repeated, here; we only give the results we need to calculate V_l^* and V_r^*.

Thus, we get the following results from [14]:

$$u^m = \frac{\rho^r u^r(\lambda^r - u^r) - \rho^l u^l(\lambda^l - u^l) + p^l - p^r}{\rho^r(\lambda^r - u^r) - \rho^l(\lambda^l - u^l)} \tag{77.a}$$

$$\rho_{l,r}^* = \rho^{l,r}\frac{(\lambda^{l,r} - u^{l,r})}{\lambda^{l,r} - u^m} \tag{77.b}$$

$$p^m = p^l + \rho^l(u^l - u^m) \times (u^l - \lambda^l) \tag{77.c}$$

$$e_{l,r}^* = \frac{\mathrm{e}^{l,r}(\lambda^{l,r} - u^{l,r}) - p^{l,r}u^{l,r} + p^m u^m}{\lambda^{l,r} - u^m} \tag{77.d}$$

Those results make it possible to calculate the intermediate states, U_l^* and U_r^*.

Now, we utilize those results to calculate V_l^* and V_r^*. Writing the Rankine–Hugoniot conditions, for the variable V, across the left wave, λ^l, that connects the state V_l^* with V_l we get the relations:

$$g_1^l \equiv (\rho u)_x|_l^* - \lambda^l \rho_x|_l^* = (\rho u)_x^l - \lambda^l \rho_x^l \tag{78.a}$$

$$g_2^l \equiv (\rho u^2 + p)_x|_l^* - \lambda^l(\rho u)_x|_l^* = (\rho u^2 + p)_x^l - \lambda^l(\rho u)_x^l \tag{78.b}$$

$$g_3^l \equiv \{u(e+p)\}_x|_l^* - \lambda^l e_x|_l^* = \{u(e+p)\}_x^l - \lambda^l e_x^l \tag{78.c}$$

Identical relations are obtained across the right wave, λ^r, that connects the state V_r^* with V_r.

Then, using $[u] = 0$ into (78.a), we get the first equation:

$$\rho_x|_{l,r}^* = \frac{g_1^{l,r} - (\rho u_x)^m}{u^m - \lambda^{l,r}} \tag{79.a}$$

Introducing this result into (78.b) and using $[u] = [p_x] = 0$, we get:

$$(\rho u_x)^m = \frac{g_2^r - g_2^l + u^m(g_1^l - g_1^r)}{\lambda^l - \lambda^r} \tag{79.b}$$

Re-introducing (79.b) into (78.b), gives:

$$p_x^m = g_2^l + u^m(\lambda^l - u^m) \times \rho_x|_l^* + (\lambda^l - 2u^m) \times (\rho u_x)^m \tag{79.c}$$

Finally, using those results into (78.c), gives:

$$e_x|_{l,r}^* = \frac{\{g_3^{l,r} - u_x(e+p)|_{l,r}^* - u^m p_x^m\}}{(u^m - \lambda^{l,r})} \tag{79.d}$$

All the remaining variables can be deduced from the relations, above.

Therefore, relations (77) and (79) permit to calculate $\widetilde{U}_l^*$ and $\widetilde{U}_r^*$, knowing $\widetilde{U}_l$ and $\widetilde{U}_r$. Now, we can formulate the algorithm that defines the HLLC scheme for the extended Euler equations.

The two-state approximate Riemann solution given by the Hermite-HLLC scheme is the following one:

$$\widetilde{U}_{i+1/2} = \begin{cases} \widetilde{U}^l & \text{if } \lambda^l > 0 \\ \widetilde{U}^*_l & \text{if } \lambda^l \leqslant 0 < \lambda^m \\ \widetilde{U}^*_r & \text{if } \lambda^m \leqslant 0 < \lambda^r \\ \widetilde{U}^r & \text{if } \lambda^r < 0 \end{cases} \tag{80}$$

The corresponding interface flux, necessary to discretize (71), is calculated as

$$F_{i+1/2} = \begin{cases} F^l & \text{if } \lambda^l > 0 \\ F^*_l & \text{if } \lambda^l \leqslant 0 < \lambda^m \\ F^*_r & \text{if } \lambda^m \leqslant 0 < \lambda^r \\ F^r & \text{if } \lambda^r < 0 \end{cases} \tag{81}$$

with the following relations to calculate F^*_l and F^*_r:

$$\begin{cases} F^*_l = F^l + \lambda^l(\widetilde{U}^*_l - \widetilde{U}^l) \\ F^*_r = F^r - \lambda^r(\widetilde{U}^*_r - \widetilde{U}^r) \end{cases} \tag{82}$$

Finally, to completely define the Hermite-HLLC scheme, we need to precise the wave speeds, according to [15]:

$$\begin{cases} \lambda^l \equiv \min(u^l - a^l, \hat{u} - \hat{a}) \\ \lambda^r \equiv \max(u^r + a^r, \hat{u} + \hat{a}) \\ \lambda^m \equiv u^m \end{cases} \tag{83}$$

where (^) represents the classical Roe's average and $a^2 \equiv \gamma p/\rho$ is the speed of sound for a perfect gas.

In [15] it is demonstrated that this choice of acoustic wave speeds, yields a positively conservative scheme. Therefore, this conclusion remains true in our formulation, at least for the variable U. For the variable *V*, the problem of "positivity" preservation is more dubious since the notion of physically realistic states is difficult to define and to interpret for spatial derivatives.

Remark 1 (*Resolution of isolated contact discontinuities*). Suppose that the left and right states, $\widetilde{U}_l$ and $\widetilde{U}_r$, are connected by a single contact discontinuity. Then, we can write:

$$\begin{cases} u^l = u^r \equiv u \\ p^l = p^r \equiv p \\ p^l_x = p^r_x \equiv p_x \\ (\rho u_x)^l = (\rho u_x)^r \equiv \rho u_x \end{cases} \tag{84}$$

Inserting those relations into (77.b) and (77.c), we get: $p^m = p, \rho^*_l = \rho^l, \rho^*_r = \rho^r$.

Therefore, one can conclude that $U^*_l = U^l$ and $U^*_r = U^r$.

In addition, (79.a) gives: $\rho_x|^*_{l,r} = \rho_x|_{l,r}$. Therefore, we also have: $V^*_{l,r} = V^{l,r}$.

Consequently, the general solution for such a case, reads as

$$\widetilde{U}_{i+1/2} = \begin{cases} \widetilde{U}^l & x < ut \\ \widetilde{U}^r & x > ut \end{cases} \tag{85}$$

This is precisely the exact solution for an isolated contact discontinuity defined by relation (84).

Remark 2 (*Resolution of isolated shock waves*). At an isolated shock wave, the shock velocity, s, is given by the largest (or the smallest) eigenvalue of the Roe matrix [10]. For example, suppose that the shock propagates to the right, i.e. $\lambda^r \equiv s$.

Then, the Rankine–Hugoniot conditions for *U*, give:

$$\lambda^r \equiv s = \frac{(\rho u)^l - (\rho u)^r}{\rho^l - \rho^r} = \frac{(\rho u^2 + p)^l - (\rho u^2 + p)^r}{(\rho u)^l - (\rho u)^r} \tag{86}$$

Introducing those relations into (77.a), we get: $u^m = u^l$. Using this result into (77.b) and (77.c), we get: $\rho^*_l = \rho^l = \rho^*_r$ and $p^*_l = p^l = p^*_r$. Therefore, there is a single wave that connects U^l and U^r. This wave is such that

$$U_{i+1/2} = \begin{cases} U^l & x < st \\ U^r & x > st \end{cases} \tag{87}$$

This is the exact solution for an isolated shock wave that propagates at the velocity, *s*.

Now, let us consider relations for the variable, V.

If it exists an isolated shock wave connecting V^l and V^r, we have, necessarily:

$$s' = \frac{(\rho u)_x^l - (\rho u)_x^r}{\rho_x^l - \rho_x^r} = \frac{(\rho u^2 + p)_x^l - (\rho u^2 + p)_x^r}{(\rho u)_x^l - (\rho u)_x^r} \tag{88}$$

However, according to the scalar results, there are no reasons that $s' \equiv s$.

Consequently, introducing (88) into (79.b), we get the following result:

$$(\rho u_x)^m = (\rho u_x)^l + \frac{\lambda^r - s'}{\lambda^l - \lambda^r} \times A \tag{89.a}$$

Where we defined the quantity: $A \equiv (\rho u)_x^l - (\rho u)_x^r - u^l(\rho_x^l - \rho_x^r)$.

Using this result into (79.a), we get:

$$\rho_x|_l^* = \rho_x^l - \frac{(\lambda^r - s')}{(\lambda^l - \lambda^r)(u^l - \lambda^l)} \times A \tag{89.b}$$

$$\rho_x|_r^* = \frac{\rho_x^r(s' - \lambda^r) + \rho_x^l(u^l - s')}{u^l - \lambda^r} - \frac{(\lambda^r - s')}{(\lambda^l - \lambda^r)(u^l - \lambda^l)} \times A \tag{89.c}$$

Lastly, (79.c) gives the following result:

$$p_x^m \equiv p_x|_r^* = p_x|_l^* = p_x^l + \frac{(\lambda^r - s')(\lambda^l - u^l)}{(\lambda^l - \lambda^r)} \times A \tag{89.d}$$

Then, we can deduce the following statements:

- If $s' = \lambda^r$, there is a single shock wave that connects V^l and V^r: this is the exact solution for V. This discontinuity is not a δ-shock wave since it propagates at the same velocity as the discontinuity in U.
- If $s' = u^l$, then $A = 0$. Therefore, the single discontinuity that connects V^l and V^r, is a contact discontinuity, according to our definitions. This discontinuity does not coincide with the discontinuity in U. The consequence is that it can exist regions where U is continuous while V presents a discontinuity: we postulate that this solution is analogous to solution (7), defining a vacuum state, in the scalar case.
- In the general case, $s' \neq u^l$ and $s' \neq \lambda^r$. In that case, the discontinuity in V is not a contact discontinuity and does not propagate at the same velocity that the shock wave in U. Consequently, using the analogy with the scalar case, we conclude that it must appear an equivalent of the Rankine–Hugoniot deficit, $e(t)$, into the solution for V. Indeed, the Rankine–Hugoniot conditions for the variable V, (88), give for example:

$$(\rho u)_x^r - (\rho u)_x^l = \lambda^r(\rho_x^r - \rho_x^l) + (s' - \lambda^r)(\rho_x^r - \rho_x^l) \tag{90}$$

This relation means that, if it exists a shock wave in (U,V) that propagates at the velocity, λ^r, then, it necessarily exists a Rankine–Hugoniot deficit for the variable, V.

According to (90), this deficit is given by the following quantity, for the variable ρ_x:

$$(s' - \lambda^r)(\rho_x^r - \rho_x^l) \tag{91}$$

This term can be compared with the definition of $e(t)$, in the scalar case (relation (21)):

$$\frac{de}{dt} = \left(\frac{[a(u)v]}{[v]} - \frac{[f]}{[u]}\right) \times [v] \tag{92}$$

Therefore, in such a case one may think that the shock-wave, solution of (71), is probably a δ-shock wave. The possibility of such an occurrence is detailed in section that follows, by analysing some numerical properties of the Hermite-HLLC scheme.

3.3. Existence of δ-shock wave type solutions for the Hermite-HLLC solver

The scope of this analysis is limited to the transonic case: $\lambda^l < 0 < \lambda^r$.

To make this study, we extend the analysis of Section 2.2 by considering the following modified form of (72):

$$\begin{cases} \widetilde{U}_t + \mathcal{A}_\varepsilon(\widetilde{U})\widetilde{U}_x = 0 \\ \mathcal{A}_\varepsilon(\widetilde{U}) \equiv \begin{bmatrix} A(U) & 0 \\ B_\varepsilon(U,V) & A_\varepsilon(U) \end{bmatrix} \end{cases} \tag{93}$$

with the following definitions:

$$\begin{cases} A_\varepsilon(U) \equiv R\Lambda_\varepsilon R^{-1} \quad (R : \text{right eigenvectors matrix}) \\ \Lambda_\varepsilon \equiv \Lambda + \varepsilon \times Id \quad (0 < \varepsilon \ll 1) \end{cases} \tag{94}$$

where Id represents the identity matrix.

The eigenvalues of $\mathcal{A}_\varepsilon$ are the eigenvalues of $A(U)$ and $A_\varepsilon(U)$: system (93) is strictly hyperbolic.

To begin, we do not consider the contribution of the contact discontinuity. Then, to account for all the possibilities, the approximate Riemann problem, typified by the Hermite-HLLE scheme, is displayed by Fig. 10: it can exist solutions for which $[U] \neq 0$ and $[V] \neq 0$ and solutions for which $[U] = 0$ and $[V] \neq 0$ (contact discontinuities).

First, writing the conservation of U within $[0,T] \times [x^l, x^r]$ ($x^l < \lambda^l T; x^r > \lambda^r T$), we get the following classical result for the intermediate state, U^*:

$$U^* = \frac{\lambda^r U^r - \lambda^l U^l + f^l - f^r}{\lambda^r - \lambda^l} \tag{95}$$

Then, the Rankine–Hugoniot condition across the wave λ^l, gives:

$$f^* = f^l + \lambda^l (U^* - U^l) = \frac{\lambda^r f^l - \lambda^l f^r + \lambda^l \lambda^r (U^r - U^l)}{\lambda^r - \lambda^l} \tag{96}$$

Similarly, conservation of V within [0,T] × [x^l,0], gives:

$$V_l^* = \frac{\lambda_\varepsilon^l V^* - \lambda^l V^l + g^l - g^*}{\lambda_\varepsilon^l - \lambda^l} = V^l + \Delta V \tag{97}$$

with: $g^* \equiv g(U^*, V^*)$ and $\Delta V \equiv \frac{\lambda_\varepsilon^l (V^* - V^l) + g^l - g^*}{\lambda_\varepsilon^l - \lambda^l}$.

Finally, conservation within [0,T] × [x^l, x^m] ($\lambda^l T < x^m < \lambda_\varepsilon^l T$), gives:

$$g_l^* \equiv g(U^*, V_l^*) = g^l + \lambda^l (V_l^* - V^l) = g^l + \Delta g \tag{98}$$

with: $\Delta g \equiv \frac{\lambda_\varepsilon^l (g^l - g^*) + \lambda_\varepsilon^l \lambda^l (V^* - V^l)}{\lambda_\varepsilon^l - \lambda^l}$.

Therefore, we can write the generalized solution in V, for the waves situated to the left-hand side of $x = 0$:

$$\begin{cases} V_\varepsilon(x,t) = V^l + (V_l^* - V^l) \times H(x - \lambda^l t) + (V^* - V_l^*) \times H(x - \lambda_\varepsilon^l t) \\ g_\varepsilon(x,t) = g^l + (g_l^* - g^l) \times H(x - \lambda^l t) + (g^* - g_l^*) \times H(x - \lambda_\varepsilon^l t) \end{cases} \tag{99}$$

or, in another form:

$$\begin{cases} V_\varepsilon(x,t) = V^l + (V^* - V^l) \times H(x - \lambda^l t) + \Delta V \times \left\{ H(x - \lambda^l t) - H(x - \lambda_\varepsilon^l t) \right\} \\ g_\varepsilon(x,t) = g^l + (g^* - g^l) \times H(x - \lambda^l t) + \Delta g \times \left\{ H(x - \lambda^l t) - H(x - \lambda_\varepsilon^l t) \right\} \end{cases} \tag{100}$$

First, suppose that solution (U,V) of (93), is continuous. In that case, the scalar theory tells us that it cannot exist a δ-shock wave into the solution.

In the limit $\varepsilon \to 0^+$, we get, from Eq. (100):

$$\begin{cases} V_\varepsilon(x,t) \underset{\varepsilon \to 0^+}{\to} V^l + (V^* - V^l) \times H(x - \lambda^l t) + [(g^l - g^*) + \lambda^l (V^* - V^l)] \times \delta(x - \lambda^l t) \times t \\ g_\varepsilon(x,t) \underset{\varepsilon \to 0^+}{\to} g^l + (g^* - g^l) \times H(x - \lambda^l t) + \lambda^l [(g^l - g^*) + \lambda^l (V^* - V^l)] \times \delta(x - \lambda^l t) \times t \end{cases} \tag{101}$$

The absence of a δ-shock wave type solution necessarily implies that: $g_l - g_l^* + \lambda^l (V^* - V^l) = 0$, into (101).

Therefore, we obtain the following result:

$$\begin{cases} V(x,t) = V^l + (V^* - V^l) \times H(x - \lambda^l t) \\ g(x,t) = g^l + (g^* - g^l) \times H(x - \lambda^l t) \end{cases} \tag{102}$$

This is the characteristic solution for the wave, λ^l, when this one is supposed to be continuous.

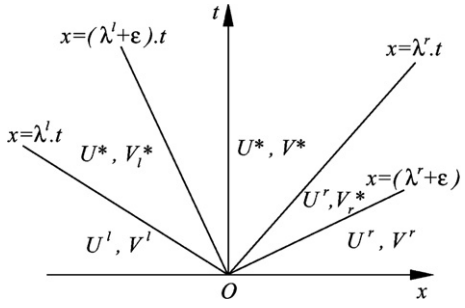

Fig. 10. Modified HLL-Riemann problem for the extended Euler equations.

Now, suppose this latter wave is a single shock wave, with a propagation speed given by λ^l, that connects (U^l, V^l) to (U^r, V^r): this means that λ^l is now solution of the Rankine–Hugoniot conditions for the variable U. Then, Eq. (100) give the following result, in the limit $\varepsilon \to 0^+$:

$$\begin{cases} V(x,t) = V^l + (V^r - V^l) \times H(x - \lambda^l t) + [(g^l - g^r) + \lambda^l (V^r - V^l)] \times \delta(x - \lambda^l t) \times t \\ g(x,t) = g^l + (g^r - g^l) \times H(x - \lambda^l t) + \lambda^l [(g^l - g^r) + \lambda^l (V^r - V^l)] \times \delta(x - \lambda^l t) \times t \end{cases} \tag{103}$$

In the general case, $g^l - g^r \neq \lambda^l (V^l - V^r)$, since the discontinuity in V does not necessarily propagate at the same velocity as the one in U. Therefore, the Dirac term in (103) do not disappear.

The term $\{g^l - g^r + \lambda^l (V^r - V^l)\}$ in front of the Dirac term is the analogous of $e(t)$ in (19) and (21). Consequently, we call this term the "Rankine–Hugoniot deficit", for the variable, V. Relations (103) tell us that the Hermite-HLLE scheme we derived, is compatible with the existence of δ-shock waves into the asymptotic solution of (93).

To end this analysis, suppose, now, that it exists a single contact discontinuity that connects (U^l, V^l) to (U^r, V^r). Furthermore, we suppose that this wave propagates to the left, at the velocity, λ^m.

Then, Eq. (100) give the following asymptotic result, for the variable V:

$$\begin{cases} V(x,t) = V^l + (V^r - V^l) \times H(x - \lambda^m t) + [(g^l - g^r) - \lambda^m (V^l - V^r)] \times \delta(x - \lambda^m t) \times t \\ g(x,t) = g^l + (g^r - g^l) \times H(x - \lambda^m t) + \lambda^l [(g^l - g^r) - \lambda^m (V^l - V^r)] \times \delta(x - \lambda^m t) \times t \end{cases} \tag{104}$$

Since we defined, in Section 3.2, the contact discontinuity in V, such that: $g^l - g^r = \lambda^m (V^l - V^r)$, we get the final result:

$$\begin{cases} V(x,t) = V^l + (V^r - V^l) \times H(x - \lambda^m t) \\ g(x,t) = g^l + (g^r - g^l) \times H(x - \lambda^m t) \end{cases} \tag{105}$$

Therefore, the Hermite-HLLC scheme we constructed, does not interpret the contact discontinuity as a δ-shock wave solution. This result is in agreement with the scalar results.

To conclude, the Hermite-HLLC scheme we derived is compatible with properties of weakly hyperbolic systems such as the extended 1D Euler equations. Despite a lack of theoretical results, we demonstrated that the numerical scheme tolerates the existence of singular solutions containing Dirac measures. However, one must note that there are no guarantees that the numerical solution is the correct entropy solution, at least for the linear variable, V.

The Hermite-HLLC scheme is typified by relations (81)–(83). Eqs. (77) and (79) enable to calculate the intermediate states $(\widetilde{U}_l^*, \widetilde{U}_r^*)$.

Now, to study the numerical behaviour of this scheme, we present some numerical experiments in the section that follows.

3.4. Numerical experiments: the 1D Euler equations

As previously noticed, there are no theoretical results concerning δ-shock wave solutions for the 1D Euler equations. Therefore, the convergence properties to the entropy solution are difficult to check. Similarly, the nature of the exact solution for the linear component V of (71), becomes difficult to interpret in general cases. For this reason – except for some simple cases that we present below – we mainly give results for the non-linear part of the solution of (71), namely, U.

In order to extend the HLSM procedure defined in the scalar case, the conservative point values $(U_{i+1/2}^{l,r}, V_{i+1/2}^{l,r})$ are calculated from the interpolated primitive variables $[\rho_{i+1/2}^{l,r}, u_{i+1/2}^{l,r}, p_{i+1/2}^{l,r}]^t$ and $[(\rho_x)_{i+1/2}^{l,r}, (u_x)_{i+1/2}^{l,r}, (p_x)_{i+1/2}^{l,r}]^t$. Those variables are interpolated by using the HLSM procedure developed in the scalar case. Although the choice of primitive variables is not referenced in the literature as the best one for dealing with one-dimensional problems (a characteristic-wise reconstruction would be more suitable) it has the advantage of being general since its extension to multi-dimensional problems is straightforward.

Unless mentioned, all the test-cases that follow are run with $\alpha = 2.5$. This value is selected as the best compromise for the cases investigated.

The computations are run on a uniform mesh ($\Delta x_i \equiv Cte$), except for the last test-case (the transonic nozzle). N grid points are utilized to discretize the equations.

The CFL number is defined as

$$\mathrm{CFL} \equiv \Delta t \times \frac{\max_i(|u_i| + a_i)}{\Delta x}$$

We choose $CFL = 0.50$ for almost all test cases, except for the accuracy tests.

Example 1 (*Accuracy tests: smooth solution*). We solve the extended Euler equations, (71), into the domain [0,2]. The initial condition is set to be: $\rho(x, t = 0) = 1 + 0.2 \times \sin(\pi x)$, $u(x, t = 0) = 1$, $p(x, t = 0) = 1$, with a 2-periodic boundary condition. The numerical solution is computed up to $t = 2$, with $\Delta t = O(\Delta x^2)$. The errors and numerical orders of accuracy for the density, ρ and its first derivative, ρ_x, obtained with the Hermite-HLLC scheme, are shown in Tables 7 and 8. As one can note it, the scheme reaches its theoretical order of accuracy both for the variable and its derivative.

Table 7
One-dimensional Euler equations

N	L_1 error	L_1 order	L_∞ error	L_∞ order
10	4.42×10^{-3}	–	3.45×10^{-3}	–
20	1.04×10^{-4}	5.4	8.13×10^{-5}	5.3
40	2.70×10^{-6}	5.2	2.12×10^{-6}	5.2
80	7.55×10^{-8}	5.2	5.93×10^{-8}	5.1
160	2.23×10^{-9}	5.1	1.88×10^{-9}	5

$\rho(x, t = 0) = 1 + 0.2 \times \sin(\pi x)$, $u(x, t = 0) = 1$, $p(x, t = 0) = 1$ Hermite-HLLC ($\alpha = 2.5$) scheme with periodic boundary conditions $t = 2$; $\Delta t = \Delta x^2/2$; L_1 and L_∞ errors of density ρ.

Table 8
One-dimensional Euler equations

N	L_1 error	L_1 order	L_∞ error	L_∞ order
10	1.48×10^{-2}	–	1.16×10^{-2}	–
20	1.06×10^{-3}	3.8	8.34×10^{-4}	3.8
40	8.87×10^{-5}	3.6	6.96×10^{-5}	3.6
80	6.59×10^{-6}	3.8	5.18×10^{-6}	3.8
160	4.52×10^{-7}	3.9	3.55×10^{-7}	3.8

$\rho_x(x, t = 0) = 0.2 \times \pi \times \cos(\pi x)$, $u_x(x, t = 0) = 0$, $p_x(x, t = 0) = 0$ Hermite-HLLC scheme with periodic boundary conditions $t = 2$; $\Delta t = \Delta x^2/2$; L_1 and L_∞ errors of density ρ_x.

Example 2 (*Steady contact discontinuity* [16]). We solve the extended Euler equations, (71), with the initial data:

$$(\rho, u, p)^l = (1.4, 0, 1) \quad \forall x \leqslant 0.5, \quad (\rho, u, p)^r = (1, 0, 1) \quad \forall x > 0.5$$

We use $N = 100$ grid points and compute the solution until a final time $t = 2$. Results are depicted in Fig. 11. It is gratifying to note that the Hermite-HLLC scheme yields a clean jump in ρ, Fig. 11(a). Similarly, this discontinuity is correctly interpreted in what concerns the variable ρ_x, Fig. 11(c): this result is in agreement with the theoretical definition we gave for a contact discontinuity, solution of the extended Euler equations. Fig. 11(b) and (d) show numerical results obtained with the Hermite-HLLE scheme: clearly, the introduction of the contact discontinuity into the Riemann solver has a strong impact, both for the variable and its first derivative.

Example 3 (*Moving contact discontinuity* [16]). The initial data are now:

$$(\rho, u, p)^l = (1.4, 0.1, 1) \quad \forall x \leqslant 0.5, \quad (\rho, u, p)^r = (1, 0.1, 1) \quad \forall x > 0.5$$

The numerical solution is computed for $N = 100$ grid points at time $t = 2$. Fig. 12 displays numerical results. Now, the numerical viscosity introduced by the reconstruction scheme smears the results. However, the Hermite-HLLC solution, Fig. 12(a) and (c), is less dissipative than the Hermite-HLLE version of the scheme, Fig. 12(b) and (d). Therefore, the dissipative nature of the method is not only the consequence of the monotonicity constraints introduced into the reconstruction, but are also due to the choice of the approximate Riemann solver.

Example 4 (*Toro's Riemann problem* [16]). Initial data are

$$(\rho, u, p)^l = (1., -19.59745, 1000) \quad \forall x \leqslant 0.8, \quad (\rho, u, p)^r = (1.0, -19.59745, 0.01) \quad \forall x > 0.8$$

The numerical solution is computed for $N = 100$ (ρ) and $N = 500$ (ρ_x, p_x) grid points at time $t = 0.012$.

For those results, we had to increase the monotonicity parameter, α, up to the value 10, in order to reduce numerical oscillations in the first derivatives, oscillations which arise close to the discontinuities. The solution of this problem consists of a rarefaction wave travelling to the left, a stationary contact discontinuity and a shock wave travelling to the right. Numerical results are depicted in Fig. 13.

Fig. 13(a), (c) and (e) present numerical results obtained with the Hermite-HLLC scheme while Fig. 13(b), (d) and (f) display those obtained with the Hermite-HLLE scheme.

Once again, the contact discontinuity is correctly captured by the HLLC version of the scheme, Fig. 13(a). This is also true for the numerical results obtained for ρ_x, Fig. 13(c). Indeed, the numerical solution for ρ_x exhibits two discontinuities: a stationary contact discontinuity, located at $x = 0.80$, and a δ-shock wave, Fig. 13(c), situated at $x = 0.85$. Fig. 13(e) displays results for the pressure gradient variable, p_x; clearly, this quantity is constant across the discontinuity located at $x = 0.80$: this fact confirms that this discontinuity is a contact wave according to the definition we gave in Section 3.3. However, in contrast with that definition, this discontinuity does not seem to be bounded: this discrepancy shows us that all the possible solutions for the extended Euler equations are not addressed yet.

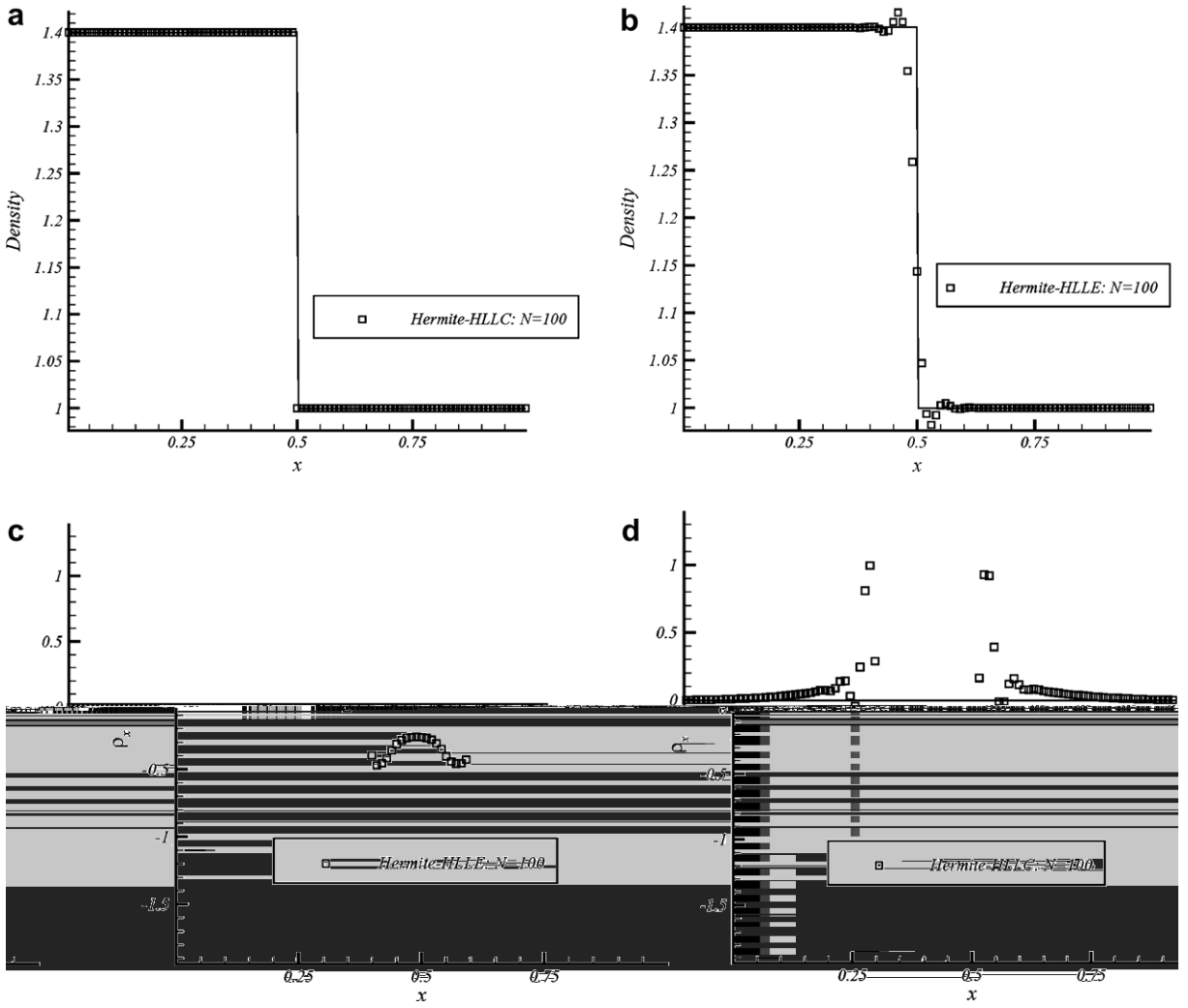

Fig. 11. One-dimensional Euler equations. Riemann problem: stationary contact discontinuity. $(\rho, u, p)^l = (1.4,0,1)$ if $x < 0.5$;$(\rho, u, p)^r = (1,0,1)$*if* $x > 0.5$. $N = 100$, $t = 2$, CFL = 0.5 (a) Hermite-HLLC scheme: $\rho(x)$, (c) $\rho_x(x)$, (b) Hermite-HLLE scheme: $\rho(x)$ and (d) $\rho_x(x)$.

Although the numerical results are more dissipated, the tendencies are left unchanged if one uses the Hermite-HLLE scheme, instead, Fig. 13(b), (d) and (f).

When the mesh is refined, both schemes converge to the same solution and the contact discontinuity is unbounded, contrarily to the conclusions we drew in Section 3.3.

Since the test cases that follow are more complicated and there are no theoretical results available for the linear variable of the extended system, (71), we only give numerical results for the non-linear variable, namely, U. However, since U and V are coupled into (71), good results obtained for U are also a consequence of a nice computation of the variable, V.

Example 5 (*Toro's Riemann problem [16]*). Initial data are

$$(\rho, u, p)^l = (1., -2, 0.4) \quad \forall x \leqslant 0.5, \quad (\rho, u, p)^r = (1., 2, 0.4) \quad \forall x > 0.5$$

The numerical solution is computed for $N = 100$ grid points at time $t = 0.15$. Fig. 14 displays numerical results. The solution of this test consists of two symmetric rarefaction waves and a contact wave. The intermediate region between the rarefaction waves is close to vacuum. As one can note it, this region is correctly computed by the Hermite-HLLC scheme, Fig. 14(left). The same conclusion is true for the Hermite-HLLE scheme except for the velocity profile that is slightly attenuated in the vacuum region, Fig. 14(right).

In regions of smooth solution, one can note the high-order accuracy of the method that is especially visible in the distortion of the pressure and density profiles. When the mesh is refined, this distortion rapidly decays.

In what follows, both schemes (Hermite-HLLE and Hermite-HLLC) share a similar behaviour: for this reason, we only show numerical results concerning the HLLC version.

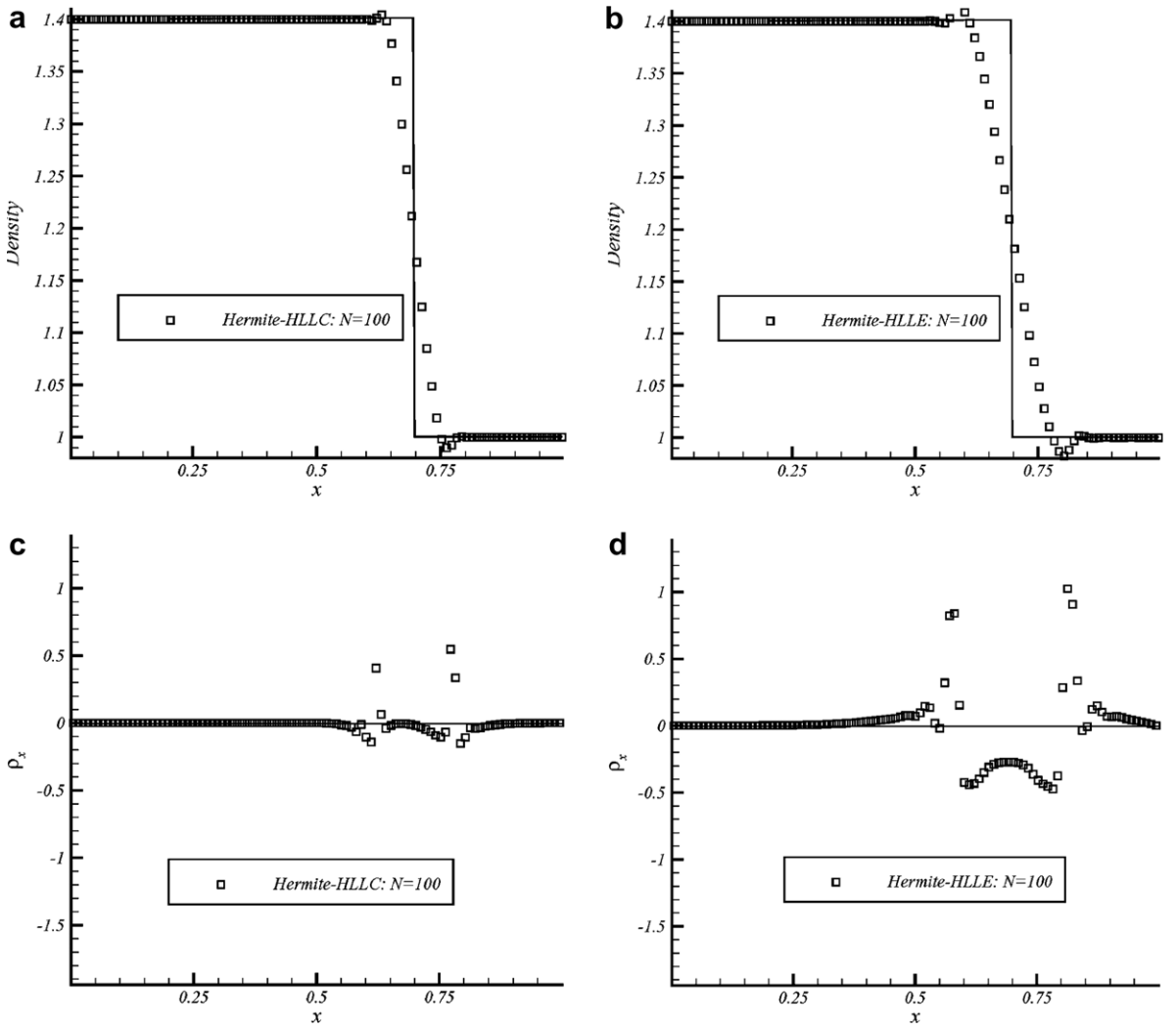

Fig. 12. One-dimensional Euler equations. Riemann problem: moving contact discontinuity. $(\rho,\ u,\ p)^l = (1.4,0.1,1)$ if $x < 0.5$; $(\rho,\ u,\ p)^r = (1,0.1,1)$ if $x > 0.5$.$N = 100$, $t = 2$, CFL = 0.5 (a) Hermite-HLLC scheme: $\rho(x)$, (c) $\rho_x(x)$, (b) Hermite-HLLE scheme: $\rho(x)$ and (d) $\rho_x(x)$.

Example 6 (*Sod's Problem*). The Sod problem is defined by the following left- and right-initial states:

$$(\rho,u,p)^l = (1.,0.75,1.) \quad \forall x \leqslant 0.3, \quad (\rho,u,p)^r = (0.125,0,0.1) \quad \forall x > 0.3$$

$N = 100$ grid points are used to discretize the computational domain. The solution is run up to $t = 0.20$. We can see that the Hermite-HLLC scheme performs reasonably well, Fig. 15. The shock wave is almost free of numerical oscillations and the contact discontinuity is not too much smeared.

In the test cases that follow, we study multi-scale problems. Therefore, to get the best accuracy possible, we set $w_i' \equiv 0$ into formulae defining the HLSM reconstruction: this means that we only use system (51) to solve for the interpolated variables $(U_{i+1/2}, V_{i+1/2})$. The value of the monotonicity parameter, α, is unchanged.

Example 7 (*Shock interaction with entropy waves: the Shu–Osher problem [13]*). We solve the extended Euler equations, (71), with a moving Mach = 3 shock interacting with sine waves in density.

The initial condition is defined as

$$(\rho,u,p) = (3.857143,2.629369,10.333333) \quad \forall x < -4$$
$$(\rho,u,p) = (1+\delta\sin 5x,0,1) \quad \forall x \geqslant -4$$

For this test, we take $\delta = 10^{-2}$. The computed density ρ is plotted at $t = 1.8$ against the "exact" solution; this solution is a converged solution computed by the HLLC scheme with 2500 grid points. Numerical results are displayed by Fig. 16.

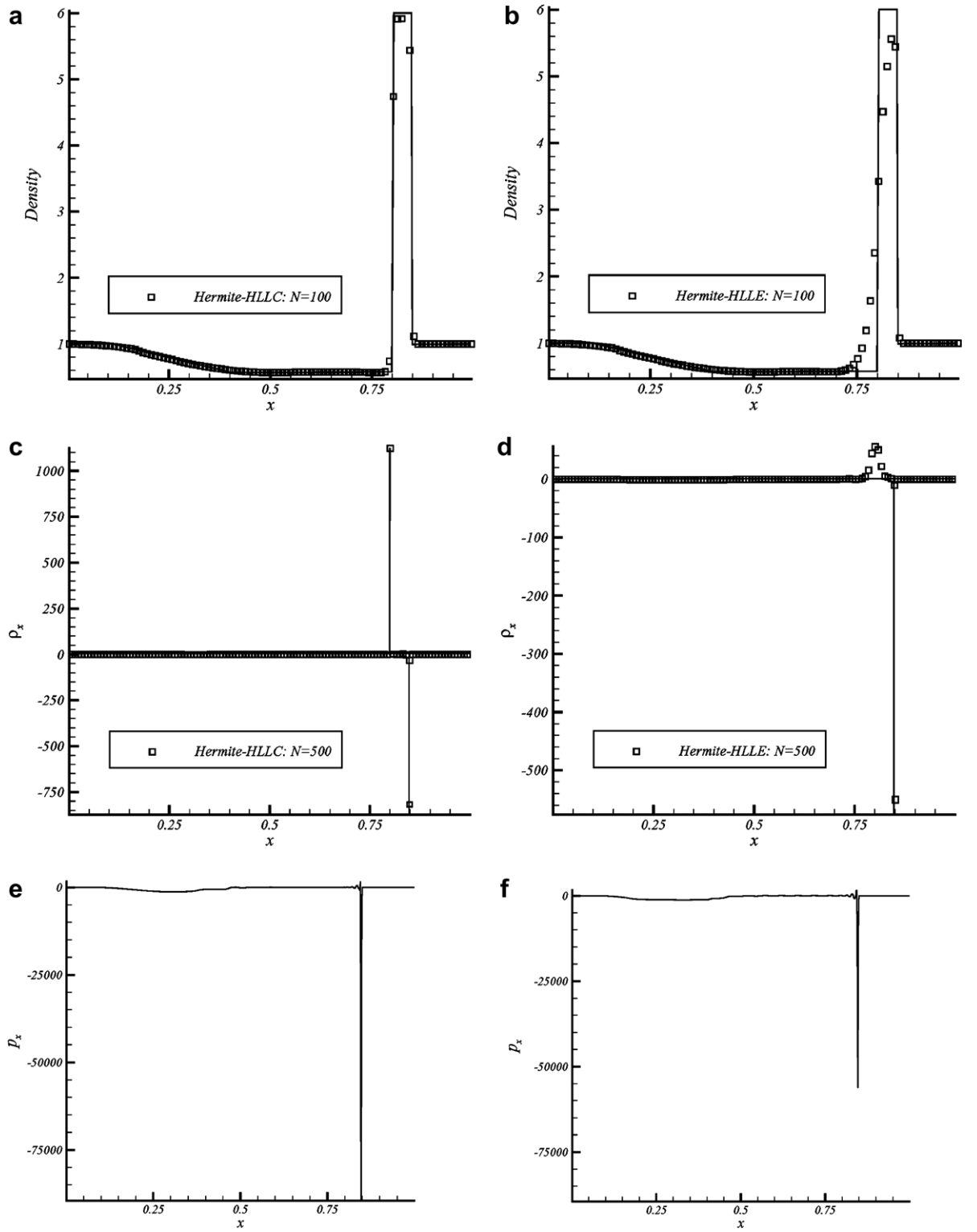

Fig. 13. One-dimensional Euler equations. Riemann problem. $(\rho, u, p)^l = (1, -19.59745, 1000)$ if $x < 0.8$;$(\rho, u, p)^r = (1, -19.59745, 0.01)$ if $x > 0.8$ $t = 0.012$, CFL = 0.5, $N = 100(\rho)$, $N = 500(\rho_x, p_x)$. (a) Hermite-HLLC scheme: $\rho(x)$, (c) $\rho_x(x)$, (e) $p_x(x)$. (b) Hermite-HLLE scheme: $\rho(x)$, (d) $\rho_x(x)$, (f) $p_x(x)$.

For $N = 300$ grid points, the shock entropy wave interaction is still underestimated. For $N = 400$ the interaction pattern is correctly predicted.

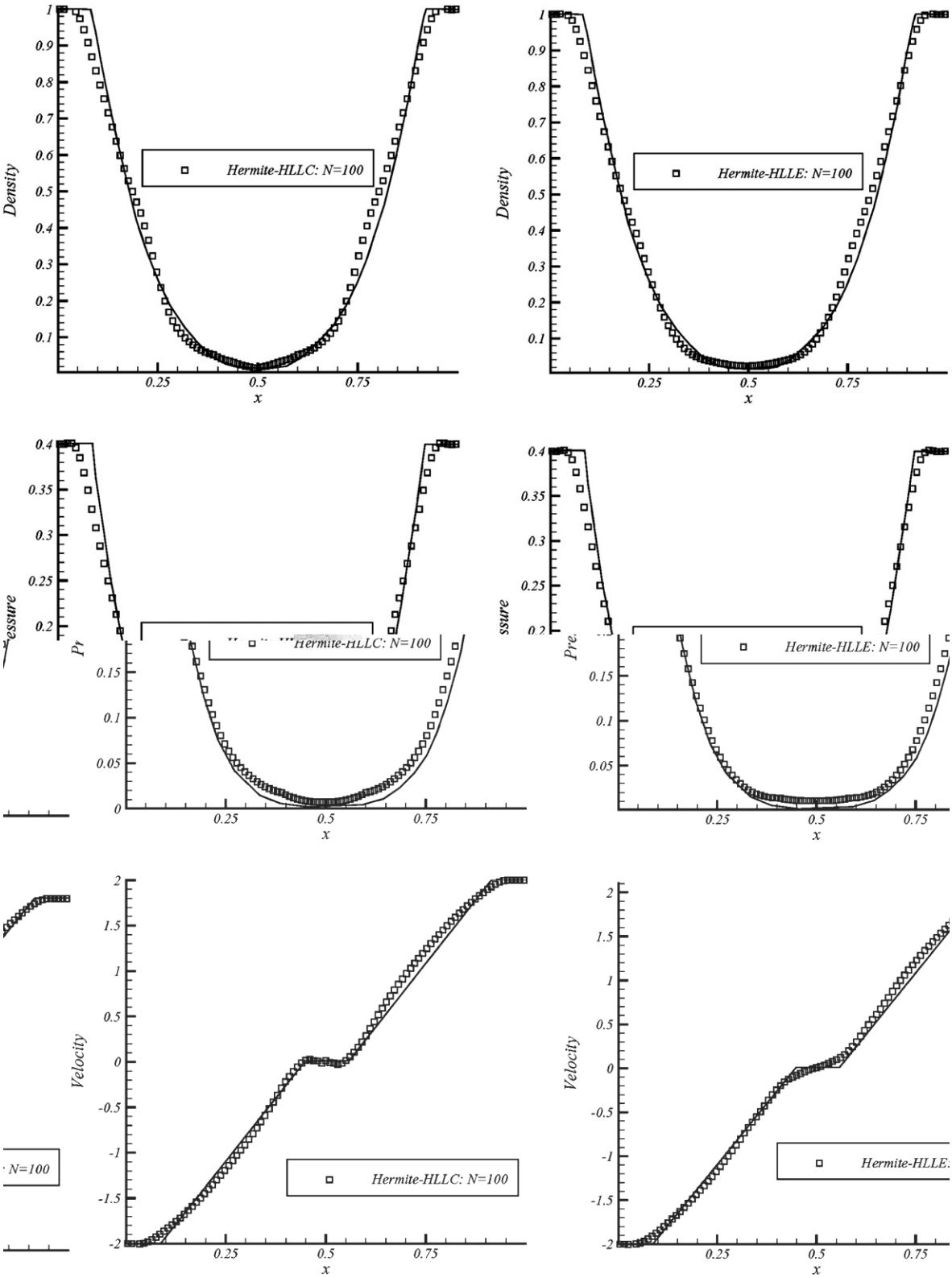

Fig. 14. One-dimensional Euler equations. Riemann problem. $(\rho, u, p)^l = (1., -2, 0.4)$ if $x < 0.5$; $(\rho, u, p)^r = (1, 2, 0.4)$ *if* $x > 0.5$ $N = 100$, $t = 0.15$, CFL = 0.5. Left: Hermite-HLLC scheme. Right: Hermite-HLLE scheme.

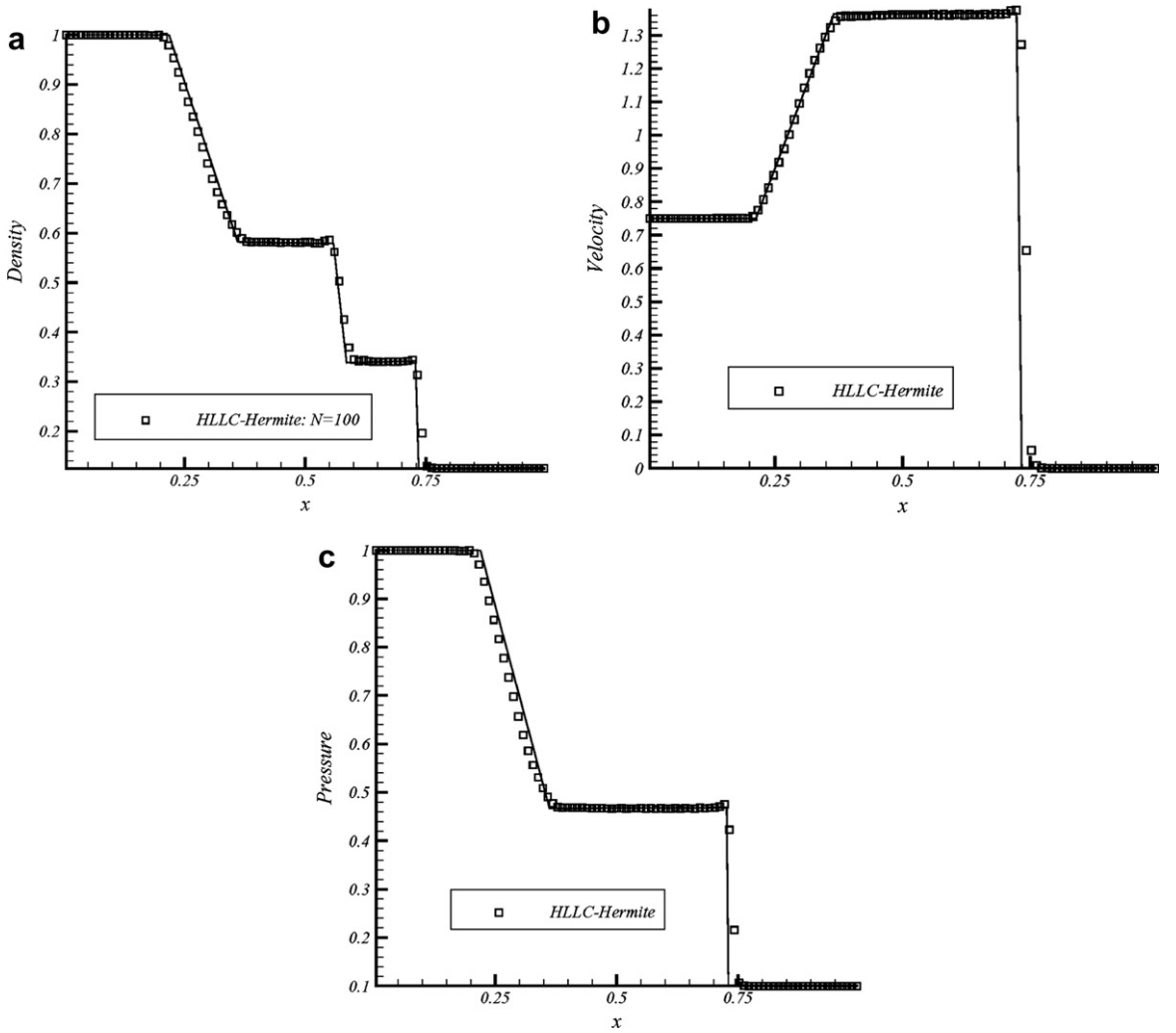

Fig. 15. The Sod problem. Hermite-HLLC scheme. $N = 100$, $t = 0.20$, $CFL = 0.5$. (a) Density, (b) velocity and (c) pressure.

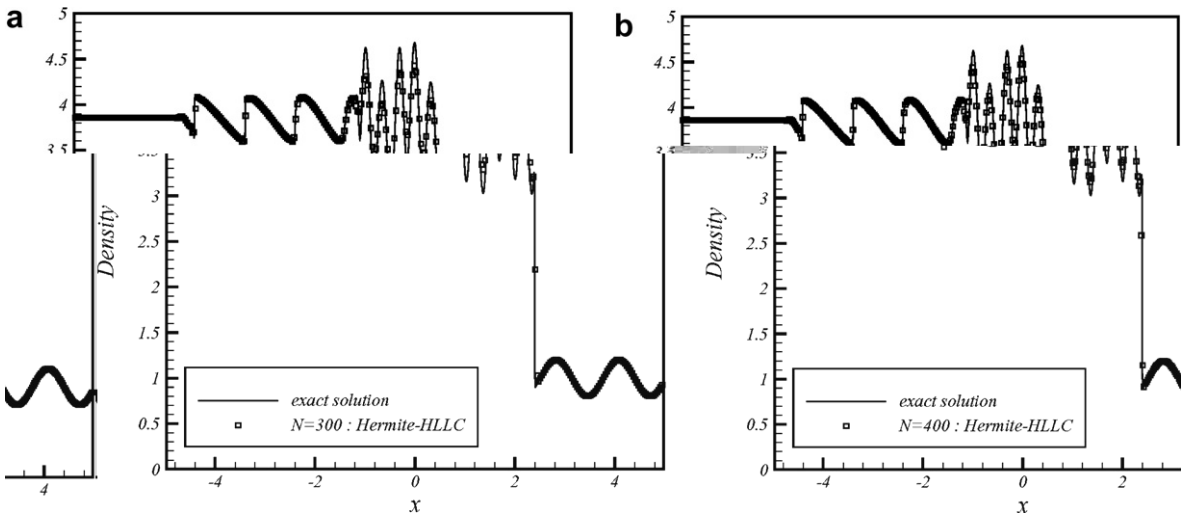

Fig. 16. Shu–Osher problem. Hermite-HLLC scheme. $t = 1.80$, $CFL = 0.5$. (a) $N = 300$ and (b) $N = 400$.

Example 8 (*Shock entropy wave interactions [17]*). This problem is very suitable for high-order shock-capturing schemes because both shocks and complicate smooth flow features co-exist. In this example, a moving shock interacts with an entropy wave of small amplitude.

On the domain [0,5], the initial condition is the following:

$$(\rho, u, p) = (3.857143, 2.629369, 10.333333) \quad \forall x < 1/2$$
$$(\rho, u, p) = (e^{-\varepsilon \sin(kx)}, 0, 1) \quad \forall x \geqslant 1/2$$

where ε and k are the amplitude and the wave number of the entropy wave, respectively.

The mean flow is a right moving Mach 3 shock. If ε is small compared to the shock strength, the shock will go to the right of the computational domain, at approximately the non-perturbed shock speed and generate a sound wave that travels along with the flow behind the shock. At the same time, the small amplitude, low-frequency entropy waves are generated in front of the shock. After having interacted with the shock, these waves are compressed in frequency and amplified in amplitude.

The main goal of such a test is to check if the structure of the amplified waves is not lost after having crossed the shock wave. Since the entropy wave is very weak relative to the shock, any excessive numerical oscillation or dissipation could alter the generated waves and the entropy waves.

In our computations, we take $\varepsilon = 0.01$. Accordingly, the amplitude of the amplified entropy waves predicted by a linear analysis, [18], is 0.08690716 (shown in the following figures as horizontal solid lines). The pre-shock wave number, k, is selected such that $k = 13$. In order to get rid of the transient waves due to the initialization, the numerical procedure is defined so that the shock crosses the computational domain twice. The numerical solution is examined when the shock reaches $x = 4.5$ for the second time. For those computations, the *CFL* is lowered to the value 0.250. The numerical results are shown in Fig. 17.

To begin, we use 400 grid points that is effectively 10 points in each wavelength of the generated entropy wave. We can see that the Hermite-HLLC scheme calculates the amplified entropy waves quite well, although their amplitude is still attenuated, Fig. 17(a). On a grid of 800 points, Fig. 17(b), the resolution becomes good.

Example 9 (*Propagation of sound waves through a transonic nozzle [19]*). The computation of sound propagating through a choked nozzle presents a challenging problem for a shock-capturing scheme. To reduce the complexity of the problem, but retaining the basic physics and difficulties, this propagation problem is modelled by a one-dimensional acoustic wave transmission problem, through a transonic nozzle [19].

In this problem, an acoustic wave is introduced at the nozzle inflow region and the sound wave that travels downstream through the transonic nozzle and interacts with the shock is to be calculated. The amplitude of the incoming sound wave is $\varepsilon = 10^{-5}$, which is very small compared to the mean values of the flow. The nozzle flow is modelled by the one-dimensional Euler equations with variable nozzle area:

$$\frac{\partial \mathbf{U}}{\partial t} + \frac{\partial \mathbf{F}(\mathbf{U})}{\partial x} = -\frac{1}{A}\frac{\mathrm{d}A}{\mathrm{d}x}\mathbf{U}' \tag{106}$$

$$\mathbf{U} \equiv [\rho, \rho u, \rho E]^t, \quad \mathbf{F} \equiv [\rho u, \rho u^2 + p, \rho u H]^t, \quad \mathbf{U}' \equiv [\rho u, \rho u^2, \rho u H]^t$$

The area of the nozzle is defined to be:

$$A(x) = \begin{cases} 0.536572 - 0.198086 \times \exp\left(-(\mathrm{Log}(2)\left(\frac{x}{0.6}\right)^2\right), & x > 0 \\ 1.0 - 0.661514 \times \exp\left(-(\mathrm{Log}(2)\left(\frac{x}{0.6}\right)^2\right), & x < 0 \end{cases}$$

The extended system for this problem is then deduced from (106), by deriving the equations with respect to x.

Flow variables are non-dimensionalized by using the upstream values. The velocity scale is a_∞ (speed of sound), the length scale is D (diameter of the nozzle) and the density scale is the static density, ρ_∞.

Then, the mean flow at the inlet is

$$\begin{bmatrix} \bar{\rho} \\ \bar{u} \\ \bar{p} \end{bmatrix}_{\text{inlet}} = \begin{bmatrix} 1 \\ M_\infty \\ 1/\gamma \end{bmatrix} \tag{107}$$

The Mach number at the inlet, M_∞, is 0.2006533 and the pressure at the exit, p_{exit}, is 0.6071752, so that a shock is formed inside the nozzle. The shock location is then: $x_s = 0.3729$.

Just upstream of the shock wave, the Mach number is $M_1 = 1.465$ and downstream, $M_2 = 0.714$. The pressure ratio (intensity of the shock wave) is then $p_2/p_1 = 2.337$.

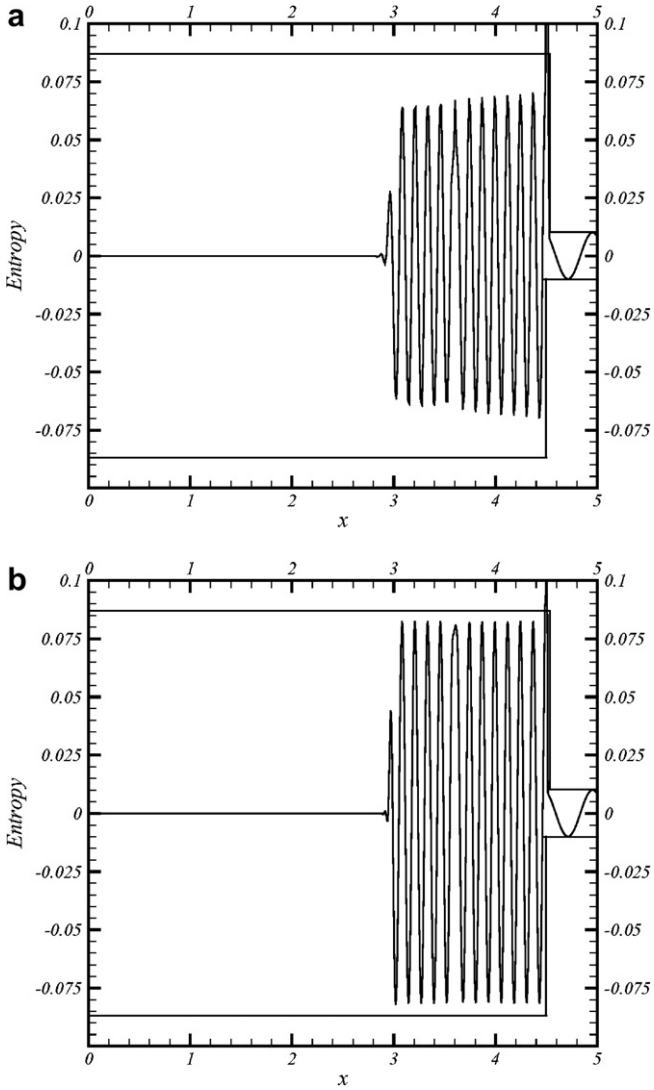

Fig. 17. Shock/entropy wave interaction: $t = 1.12687$, $k = 13$, $CFL = 0.25$. Hermite-HLLC scheme: (a) $N = 400$ and (b) $N = 800$.

The incoming acoustic wave, with angular frequency, $\omega = 0.6\pi$, is described as

$$\begin{bmatrix} \rho \\ u \\ p \end{bmatrix}_{\text{acoustic}} = \varepsilon \begin{bmatrix} 1 \\ 1 \\ 1 \end{bmatrix} \sin\left[\omega\left(\frac{x}{1+M_\infty} - t\right)\right] \tag{108}$$

The acoustic perturbations for the derivatives are derived from (108).

In the present work, the acoustic wave will be computed directly by solving the non-linear governing equations rather than solving the linearized equations (see [19] for some examples on the linearized problem). This makes it harder to compute the acoustic waves. The challenge is whether the small amplitude wave can still be captured in the computation by the Hermite-HLLC scheme. The computational domain is $-10 \leqslant x \leqslant 10$ and a non-uniform mesh, refined in the throat region, is used.

To begin, the steady state of the nozzle flow is computed. For the flow variables, using the mean exact solution of this problem specifies the initial conditions.

The derivatives are then estimated by using a centred second-order finite-difference approximation. At the boundaries, the back-pressure is specified at the outlet and the total pressure and density are specified at the inlet. The other needed information at both the inlet and outlet, are obtained using extrapolation from their neighbouring mesh points. Concerning the derivatives, all those quantities are set to zero at the inlet since the flow is assumed uniform. At the outlet, the pressure derivative is set to zero while the remaining quantities are extrapolated in order for the error to leave the computational domain without numerical reflections.

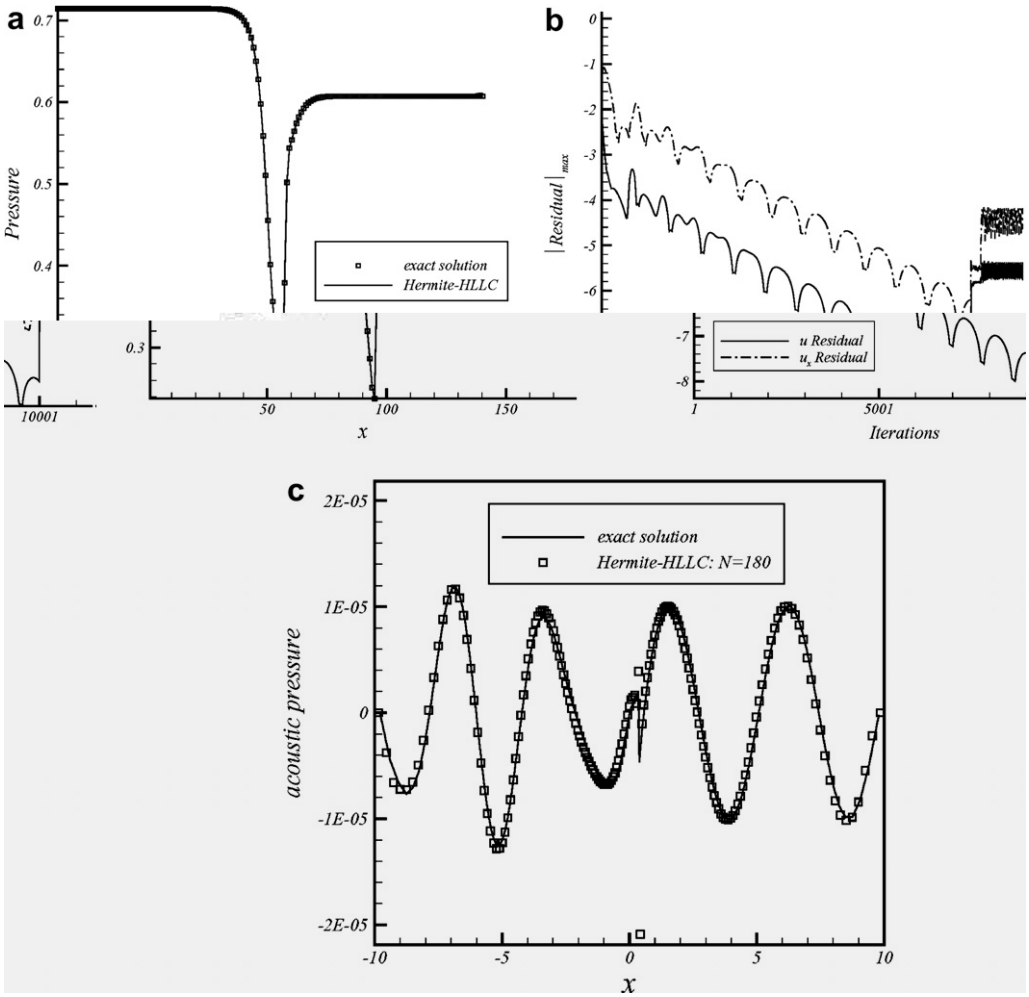

Fig. 18. Propagation of sound waves through a transonic nozzle. Hermite-HLLC scheme. $CFL = 0.80$, $N = 180$, $t = 14T$, $\Delta x_{\min}/\Delta x_{\max} = 0.19$. (a) Mean pressure, (b) maximum residual and (c) acoustic pressure.

The steady-state solution of the extended form of (106), obtained using a 180 points non-uniform mesh ($\Delta x_{\min} = 6.74 \times 10^{-2}$, $\Delta x_{\max} = 0.35$) with $CFL = 0.80$, is compared with the exact solution, Fig. 18(a). The solution is converged to machine precision, Fig. 18(b). It can be seen that flow properties are uniform in most region of the nozzle, but change dramatically near the nozzle throat, Fig. 18(a). Lastly, the shock is captured without any numerical oscillation.

After the steady-state flow-field is computed, the acoustic wave propagation can be simulated using the same non-linear solver.

First, the initial conditions are specified using the steady-state solution previously calculated. Then, at the inlet, the solution (108) is superimposed for the variables and its derivatives. Numerical solution of the acoustic pressure at $t = 14T$ is shown in Fig. 18(c). With $N = 180$ grid points, the wave pattern is correctly captured. However, the amplitude of the acoustic wave at the shock location is larger than that indicated by the analytical solution: this is due to a small error introduced by the scheme just at this place. Indeed, this error comes from the monotonicity constraint that arises at the shock location: at this place, the scheme becomes first-order and the numerical dissipation increases. Fortunately, one can note that the smooth part of the solution is not affected by this drawback: this means that the dissipative error remains local.

4. Concluding remarks

The "zero pressure gas dynamics" equations, systems that arise in non-linear geometrics or in astrophysics, extended systems of which the unknowns are the variable and its derivatives, are all weakly hyperbolic systems.

In some cases, weakly hyperbolic systems may generate "no classical" solutions containing a Dirac measure. In the scalar case, a mathematical theory was recently developed to solve the Cauchy problems in these non-standard situations.

This theory introduces new singularities, called "δ-shocks". In a δ-shock wave type solution, the non-linear component of the solution verifies the Rankine–Hugoniot conditions, while the linear part of the solution contains a Dirac function.

Relying upon these results, we developed a method that tolerates this possible singular solution. To reach this target, we first devised the so-called "Hermite-HLL" Riemann solver.

In the scalar case, we demonstrated that such a solver correctly captures the mechanism that generates a δ-shock. Thus, by adding to the Hermite-Least-Square-Monotone (HLSM) interpolation, numerical constraints for the first derivative, we got numerical results that are in close agreement with the underlying mathematical theory.

Moreover, we demonstrated that numerical oscillations that appear into the linear variable, close to singularities, could appreciably deteriorate, in some cases, the accuracy of the non-linear variable.

In a second step, we generalized the resulting scheme to the numerical approximation of the extended 1D Euler equations. To this aim, we developed the "Hermite-HLLC" scheme that introduces a third wave into the classical HLL Riemann solver. This third wave enables to discriminate between a δ-shock wave and a contact wave. In the absence of theoretical results for the Euler equations, we utilized an analogy with the results of the scalar study to define the new properties of the contact wave, solution of the extended Euler equations.

Numerical experiments about isolated discontinuities gave promising results. In addition, numerical results obtained for flow with complex patterns, demonstrated the versatility of the numerical method.

All those results are encouraging. They demonstrate that the solution of a weakly hyperbolic system can be captured, without generating spurious numerical oscillations or important dissipative terms in regions close to discontinuities.

However, those results are only partial; we did not prove the convergence to correct entropy solutions and many improvements should be made to enhance the robustness and the viability of the method. Furthermore, discrepancies with the definition we gave of a contact discontinuity, appeared in the computations (example 4).

Considering those remarks, some efforts should be made in the following fields:

- *In the mathematical field*. The theory should be extended to systems that are more complex. By defining and generalizing the concepts of "δ-shock wave" and that of entropy solution, the benefit in the quest of a well-adapted approximate solver, would be immediate. In addition, all the possible solutions for such problems would be clearly identified and referenced.
- *In the numerical field*. Two directions of research should be addressed. Firstly, the HLSM interpolation should be improved by modifying the constraints introduced to interpolate the first derivatives. Indeed, those constraints enable the capture of singularities without significant numerical oscillations; however, they also generate important dissipative terms and, consequently, they must be discarded for computing flows with complex patterns. Secondly, a fifth-order accuracy is clearly insufficient if one wishes to calculate, accurately and simultaneously, the variable and its derivatives. Accordingly, a more accurate method should be devised, by extending the numerical stencil, for example.

In spite of its limits and insufficiencies, the method we promoted has the advantage to be adaptive. First, because numerical constraints can be added or modified, easily, to monitor the monotonicity of the scheme; then, because the use of a least-square formulation enables to deal with irregular meshes. Lastly, because the Hermite-HLL procedure can be adapted, either by modifying the calculation of the characteristic wave speeds or by changing the physical definition of the contact discontinuity.

In a next future, we shall try to extend some features of this method to multi-dimensional hyperbolic problems.

Acknowledgments

The author wishes to thanks with recognition, Dr. G.B. Deng (Ecole Centrale de Nantes – France) who provided a technical support essential to this work.

References

[1] K.T. Joseph, A Riemann problem whose viscosity solutions contain delta-measures, Asymp. Anal. 7 (1993) 105–120.
[2] D. Schaeffer, M. Shearer, Riemann problems for non-strictly hyperbolic 22 systems of conservation laws, Trans. Amer. Math. Soc. 304 (1987) 267–306.
[3] D. Tan, T. Zhang, Y. Zheng, Delta-shock waves as limits of vanishing viscosity for hyperbolic systems of conservation laws, J. Diff. Eq. 112 (1994) 1–32.
[4] G.Q. Chen, H. Liu, Formation of delta-shocks and vacuum states in the vanishing pressure limit of solutions to the Euler equations for isentropic fluids, SIAM J. Math. Anal. 34 (2003) 925–938.
[5] V.M. Shelkovich, The Riemann problem admitting, shocks and vacuum states (the vanishing viscosity approach), J. Diff. Eq. 231 (2006) 459–500.
[6] H. Yang, Riemann problems for a class of coupled hyperbolic systems of conservation laws, J. Diff. Eq. 159 (1999) 447–484.
[7] V.G. Danilov, V.M. Shelkovich, Dynamics of propagation and interaction of delta-shock waves in conservation laws systems, J. Diff. Eq. 211 (2005) 333–381.
[8] E.Yu. Panov, V.M. Shelkovich, -shock waves as a new type of solutions to systems of conservation laws, J. Diff. Eq. 228 (2006) 49–86.
[9] G. Capdeville, Towards a compact high-order method for non-linear hyperbolic systems, I. The Hermite Least-Square Monotone (HLSM) reconstruction, J. Comput. Phys., submitted for publication.
[10] B. Einfeldt, C.D. Munz, P.L. Roe, B. Sjögreen, On Godunov-type methods near low densities, J. Comput. Phys. 92 (1991) 273–295.
[11] E. Weinan, Yu.G. Rykov, Ya.G. Sinai, Generalized variational principles, global weak solutions and behaviour with random initial data for systems of conservation laws arising in adhesion particle dynamics, Commun. Phys. Math. 177 (1996) 349–380.
[12] W. Sheng, T. Zhang, The Riemann problem for transportation equations in gas dynamics, Mem. Amer. Math. Soc. 137 (564) (1999).
[13] C.W. Shu, S. Osher, Efficient implementation of essentially non-oscillatory shock-capturing schemes, J. Comput. Phys. 77 (1988) 439–471.
[14] E.F. Toro, M. Spruce, W. Spears, Restoration of the contact surface in the HLL Riemann solver, Shock Waves 4 (1994) 25–34.
[15] P. Batten, N. Clarke, C. Lambert, D.M. Causon, On the choice of wavespeeds for the HLLC Riemann solver, SIAM J. Sci. Comput. 18 (1997) 1553–1570.

[16] E.F. Toro, Riemann Solvers and Numerical Methods for Fluid Dynamics, Springer-Verlag, 1997.
[17] C.-W. Shu, Essentially non-oscillatory and weighted essentially non-oscillatory schemes for hyperbolic conservation laws, ICASE Report 97-65.
[18] J. Mc Kenzie, K. Westphal, Interaction of linear waves with oblique shock waves, Phys. Fluids 11 (1968) 2350–2362.
[19] Third Computational aeroacoustics Workshop on Benchmark Problems, NASA/CP-2000-209790.
[20] J. Qiu, C.-W. Shu, Hermite WENO schemes and their applications as limiters for Runge–Kutta discontinuous Galerkin method: one-dimensional case, J. Comput. Phys. 193 (2004) 115–135.